NTNU – Trondheim
Norwegian University of
Science and Technology

Quasi-static Analyses of Slender Structures with Complex Cross-Sections using Explicit FEM Codes

Anette Wester Kyrre

Master of Science in Mechanical Engineering
Submission date: October 2013
Supervisor: Kjell H. Holthe, KT

Norwegian University of Science and Technology
Department of Structural Engineering

Institutt for konstruksjonsteknikk

FAKULTET FOR INGENIØRVITENSKAP OG TEKNOLOGI
NTNU – Norges teknisk-naturvitenskapelige universitet

MASTEROPPGAVE 2013

for

Anette Wester Kyrre

Quasi-static Analyses of Slender Structures with Complex Cross-Sections using Explicit FEM Codes

(Kvaisstatiske analyser av slanke strukturer med komplekse tverrsnitt ved bruk av eksplisitte FEM analyser)

Bakgrunn

Subsea cables and umbilicals have a very complex cross-sectional design with many different components of different materials. In the length direction the layers are twisted with different stroke lengths, so 2D analyses are not feasible. The challenging contact computations make explicit FEM codes such as ANSYS LS-Dyna and ANSYS Autodyn quite useful. However, the time scale of the physical situation that you want to simulate might make them highly time consuming due to the small time steps required by the explicit numerical solution schemes. This is the case when a static, or almost static, situation needs to be modeled. One approach to overcome this difficulty is to tweak your transient FEM analyses into a quasi-static analysis by removing dynamic effects.

Selve oppgaven

The aim for the suggested thesis is to develop a method for turning a dynamic analysis of a slender and complicated cable into a quasi-static analysis. The developed method shall ensure that the stress levels in the steel parts are calculated accurately. Further, the global stiffness parameters such as longitudinal-, torsional and bending stiffness shall be calculated and assed. The resulting analysis time (CPU-time) should be as short as possible as the method is to be used in a product development phase of the project.

One detail that is important, in addition to the global behavior, is the frictional behavior between the various cross-sectional components. For the structures in question it is known from testing that a highly distinct stick/slip point will be present in a bending test. Initial analyses have had difficulties in predicting this phenomenon correctly in an explicit computation. The current work should establish a method for predicting this phenomenon.

If relevant experiments are available in literature, simulations should be run and compared to the experiments.

Besvarelsen organiseres i henhold til gjeldende retningslinjer.

Besvarelsen skal leveres til Institutt for konstruksjonsteknikk innen 28/10 – **2013.**

Oppgaven veiledes i et samarbeid mellom selskapet EDRMedeso AS og Institutt for konstruksjonsteknikk, NTNU

Kontaktpersoner

Veileder ved EDRMedeso AS	:	Frode Halvorsen	(Frode.Halvorsen@edrmedeso.com)
Ansvarlig faglærer NTNU	:	Kjell Holthe	(kjell.holthe@ntnu.no)

NTNU, 11. juni, 2013

Kjell Holthe

Ansvarlig faglærer

Preface

This thesis concludes the work of my master project, at the Department of Structural Engineering at NTNU in the fall of 2013. I would first of all like to thank my supervisor professor Kjell H. Holthe for his guidance and advices. I would also like to thank my co-supervisor Frode Halvorsen, Ph.D, from EDR Medeso AS, for providing me with such an interesting project and for his help and guidance I have recieved during the work. A thanks goes to all of my colleagues at EDR Medeso, department of Sandvika, who has also helped me a lot with my work.

Oslo, October 24, 2013

Contents

List of Figures

List of Tables

Nomenclature

α	Lay angle
δ	Axial deformation
Δt_{cr}	Critical time step
κ	Curvature
ψ	Angular coordinate
ψ°	Slip angle
ρ	Material density
θ	Angle of the cable end
A	Tendon cross-section area
c_d	Dilatational wave speed
F_f	Friction force
L_c	Characteristic length of element
L_p	Pitch length
$M_{bending}$	Bending moment acting on the support cross section
P_y	Pressure in y direction
P_z	Pressure in z direction
Q_i	Cross-section force resultant along axis i
q_i	Line load along axis i
X^i	Coordinate along curve-linear tendon axis i
b	Tendon width
E	Young's modulus

EI	Bending stiffness
F(t)	External force
I	Area moment of inertia
L	Cable length
m	Mass
R	Mean layer radius
r	bending radius
t	Thickness
v	Velocity

1 Introduction

Flexible pipes and umbilical cables are crucial elements in floating production systems because of their slender structure and complex cross sections as well as their area of application. While umbilical cables supplies energy (electrical and hydraulic), chemical injections and bidirectional signal transmissions to remotely installed equipment, the flexible pipes transports oil and gas from wells to sub-sea components.

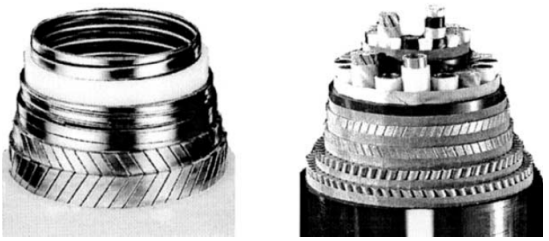

Figure 1: Flexible pipe and umbilical cable [1]

A typical flexible pipe is usually compsed of polymeric homogeneous cylindrical layers, metallic (or carbon fiber) armouring layers and reinforced interlocked metallic layers for burst and collapse strength. Umibilical cables on the other hand have homogeneous layers and metallic armours together with hydraulic hoses and cables in their central core [9] (figure1). The cables acts strong and stiff in response to internal- and external pressure, tension and torque, but in bending they are highly deformable [7].

1.1 Project Objectives

One of the main objectives in this paper is to develop a method for turning a dynamic analysis of a slender and complicated cable (umbilical) into a quasi-static analysis. Because the model set up is defined in 3D it follows that the contact computations are challenging. Therefor explicit FEM codes such as ANSYS LS-Dyna or ANSYS Autodyn shall be used.

This overall main objective may be divided into more specific objectives such as:

- Perform a literature review on theoretical and experimental studies of stresses in flexible pipes as well as the influence of bending stick-slip behaviour
- Develope a 3D model set up of a flexible cable and make use of the explicit FEM codes of ANSYS LS-Dyna and ANSYS Autodyn to study the following
  - **Global stiffness parameters** such as longitudinal-, torsional and bending stiffness
  - Investigate how to **predict the stick-slip phenomenon** as correctly as possible, as well as investigate if a stick-slip behavior is present during bending.
  - Present and assess the **resulting analyses times** (CPU-time) of the models developed.

1.2 Project structure

To achieve the above mentioned objectives, the modeling will be carried out in a specific manner. This is because of the complexity associated with modeling umbilical cables and because a quasi-static approach is sought.

A model of a umbilical cable can be considered large, hence the turn around time may be very long. To practice intelligent use of the system resources to minimize the CPU time and the number of increments, there exists several techniques. These might be sub modeling, history output filtering, restart of analysis and/or simplifications of the model. In this case, simplification of the model will be carried out by simplification of the geometry.

The complexity of a umbilical cable is situated in the cross section of the cable, which is why the analyses in this thesis starts with modeling a simple flexible cable of structural steel. Further complexity is added gradually, which will involve modeling one tendon wound around a inner sheath, and supported by another sheath on the outside.

To be able to analyse a possible stick-slip behavior of the tendon during bending, a friction element is first modeled. This is only to obtain knowledge of the contact tools available in ANSYS LS-Dyna, as well as the friction behavior between two flexible solid elements in contact. Hence, a model like this will not mainly be part of the results associated with the project objectives, but acts as an auxiliary model.

After analysing the model with one tendon, and comparing the results with relevant theory presented in the literature review, even more complexity is added to form another model. This last model consists of two armouring layers with 30 tendons at each layer, wound around a inner sheath and supported by another sheath on the outside as before.

In the section $\ll$ Model set up $\gg$ the four models now mentioned will be presented in details, followed up by the results found during the analyses. The final results will thereafter be discussed in a separate section. The final turn around time of all the models is the a main focus during the whole process from the model set up to the analyse settings.

2 Literature Review

2.1 Quasi-static modelling of a dynamic problem

It is seen that in engineering research, Finite Element Method (FEM) is a popular computational tool, and one can basically choose between an implicit or explicit approach. In practical applications, important differences between the two methods is related to
stability and economy.

As mentioned in section 1.1 explicit FEM codes will be used, and if applying explicit dynamics to model quasi-static events, special considerations need to be taken in to account. Firstly, looking at a models natural time period is computationally impractical becuase it requires literally millions of time increments. To be able to obtain an economical solution it is therefor necessary to artificilally increase the speed of the process in the simulation while keeping the inertia forces insignificant. Mass scaling and change of loading rates are amoung techniques that can help reduce the simulation time.

One way of evaluating whether or not the results from an explicit simulation reflect a quasi-static solution, is to examin the energy content provided. The kinetic energy should not exceed a small fraction, typically 1-5%, of the internal energy produced through the main part of the analysis.

2.2 Mass Scaling

With mass scaling it is possible to increase the size of the stable time increments, hence reduce the simulation time. But, this may come at the expense of making the inertia forces more dominant.

The explicit scheme is given to be conditionally stable [4], but one must take in to account that there excist a critical time step Δt_{cr} that must not be exceeded if mass scaling is implemented. Otherwise the explicit integration scheme fails and becomes unstable. On the other hand we do not want a time step that is to small as it makes the calculations too expensive. The critival time step is defined by:

$$\Delta t_{cr} = \frac{L_e}{c_d}, \qquad \text{where} \qquad c_d = \sqrt{\frac{E}{\rho}} \tag{1}$$

Since changes in characteristic length and density of each element effets the size of the time increment, it is important to mesh the model right. In ANSYS, the time step used in an explicit dynamic analysis is constrained to maintain stability and consistency via the CFL (Courant-Friedrichs-Levy) condition, that is, the time increment is proportional to the smallest element dimension in the model and inversely proportional to the sound speed in the materials used [2].

2.3 Hourglass mode

When making use of reduced integration eight node hexahedral elements in explicit dynamics (which is done in this project) "hourglass" modes of deformation, also called zero energy modes, may occur. The strain rates and forces associated with hexahedral elements only involve differences in velocity and/or coordinates of diagonally opposite corners of the elements.

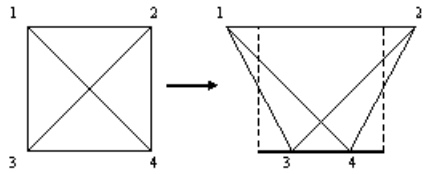

Figure 2: Example of distortion [2]

If an element distort in such way that if the above mentioned differences remains unchanged, the strain will not increase within the element hence resistance to distortion will not be present. This is illustrated in figure 2 where the two diagonals in the element to the left has the same lengths as in the element to the right, even though the element distorts.

According to ANSYS 15.4 help system [2], it is possible to correct the presence of hourglass instabilities in two ways, either by applying AUTODYN Standard- or Flanagan Belytschko settings.

- **AUTODYN standard** is often refereed to as a viscous formulation, and generates hourglass forces proportional to nodal velocity differences
- **Flanagan Belytschko** is invariant under rigid body rotation, and is recommended if large rotations of hexahedral elements are expected.

It is worth noting that the sum of the hourglass forces applied to an element to correct its undesired behaviour is normally zero, and therefor the momentum of

the system is unaffected by these forces. However, they act on the nodes of the elements which implies why the energy associated with hourglass forces is stored locally in the specific internal energy of the element.

2.4 The stick-slip phenomenon

Even though friction is common in mechanical systems, it is one of the most challenging physical effects to include in an overall model. The two main reasons for this is the difficulties associated with representing the interaction between two surfaces generatating friction and the stick-slip phenomenon occurring due to this interaction [6].

The basic understanding of stick-slip is that when two element are sliding relative to each other, a spontaneous jerking motion occures. A simple example of a stick slip situation is illustrated in the figure below

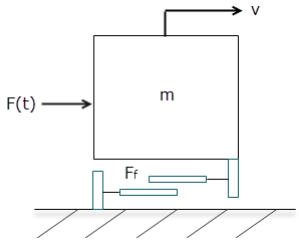

Figure 3: Simple Stick Slip Example

If the external force exceeds some breakaway force (i.e. static friction force) and a relative velocity exists between the element and the ground, a sudden jump in the velocity of the movement occurs and the element slides along the ground. A friction force is then generated to oppose this motion, which can be assumed to be nearly constant or mildly dependent on the relative velocity.

If the relative velocity approaches zero, the element that previously was in motion starts to 'stick' to the ground, and will finally stop moving, having virtually zero relative velocity. The element will remain still until a force can exceed the breakway force, and a sliding motion begins again. In other words, the element may be alternating between sticking to the ground and sliding over it.

2.5 The bending stick-slip model

The modeling approach of a umbilical cables subjected to bending as well as the moment-curvature modeling of bending stick-slip behavior is the main topic of this subsection. In literature, these topics have been less focused on by only a few authors. Work done in [9] by Professor Svein Sævik from the Institute of Marine Technology at NTNU will therefor provide the main motivation for further investigation in this paper.

The axisymmetric bending model described in [9] is defined such that stresses due to elastic bending of each tendon and friction stick-slip behavior between layers can be described. This is initially done on element level and then implemented into a standard beam finite element, a formulation that is referred to as the moment model (MM). Although umbilicals undergoes large rigid body motions induced i.e. ocean waves, the associated strains are within the elastic range of material behavior and remain small.

According to [8], during one bending cycle the transverse tendon displacement is rather small. Because of this we can assume that each tendon follows a loxodromic curve which implies no transverse slip. In other words, the initial path of each tendon is kept constant during bending.

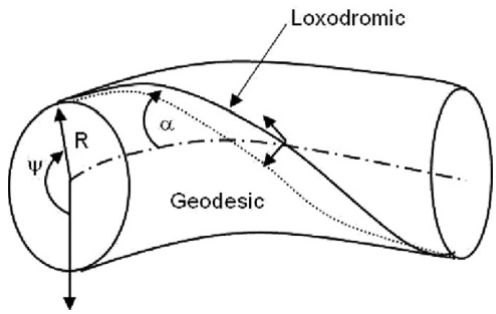

Figure 4: Loxodromic and geodesic curves [9]

Further by assuming that the contact pressure and friction is constant along the loxodromic path, both the resulting friction and contact pressure will be influenced by the curvature [9] in terms of change in helix curvature and increase of stress that results from friction.

At a certain point during the increased bending, slip will occur between layers

because the shear stress at the neutral axis of bending exceeds the shear capacity governed by friction. If we consider an arbitrary cross-section subjected to bending about Z^2, one part of the cross-section will be in a stick-region and the other part will be in a slip-region. This is illustrated in the figure below.

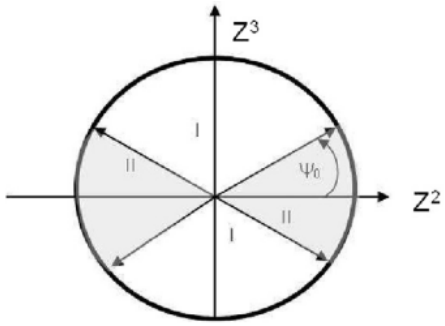

Figure 5: Stick-Slip regiones of a cross-section [9]

where region I is the stick domain, and region II is the slip domain. The transition between these two regions is described by the the angle

$$\psi_0 = \cos^{-1}\left(\frac{\beta_{2c}}{\beta_2}\right) \tag{2}$$

where β_{2c} is the critical curvature and β_2 is the bending curvature during plane deformation. Because we assumed that all the tendons are moving
harmonically it is considered valid to use the critical curvature to estimate the start slip curvature.

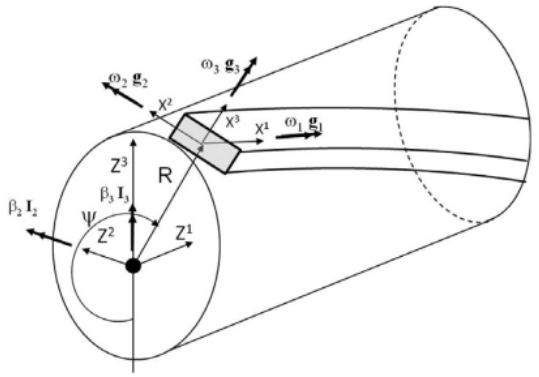

Figure 6: Global and local element curvature quantities [9]

2.5.1 Critical curvature

Considering plane deformation only, the axial force Q_1 in the tendon before slip is given by

$$Q_1 = -EA\cos^2\alpha R\cos\psi\beta_2 \tag{3}$$

The associated shear force q_1 per unit length along the tendon is given by

$$q_1 = EA\cos^2\alpha\sin\alpha\sin\psi\beta_2 \tag{4}$$

is found by differentiating equation 3 by the length coordinate X^1 and applying the relation $\psi = \frac{\sin\alpha}{R}X^1$.

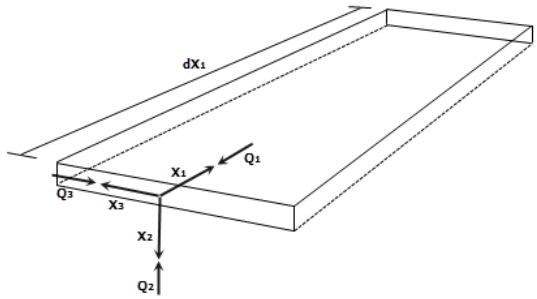

Figure 7: Simple coordinate system of an infinitesmall tendon element

Knowing this, it is possible to define the critical curvature β_{2c} by equating 4 by the maximum possible shear stress q_{1c}

$$\beta_{2c} = \frac{q_{1c}}{EA\cos^2\alpha\sin\alpha} \tag{5}$$

2.6 Global stiffness parameters

2.6.1 Axial stiffness

The axial stiffness of a cable is its resistance of being compressed or elongated by an axial force, and is found by

$$k_{axial} = \frac{LF(t)}{\delta} \tag{6}$$

2.6.2 Bending stiffness

When cables are subjected to bending, the determination of the bending stiffness is of importance. Even though it basically is a 'defined' (auxiliary) quantity, it helps you understand the bending process because it is based on a combination of cross-sectional- and material values.

The bending stiffness is found from the relationship between applied bending moment ΔM and the resulting curvature $\Delta\kappa$ of a cable, and is given by

$$k_{bending} = EI = \frac{\Delta M_{bending}}{\Delta\kappa_{bending}} \tag{7}$$

where the area moment of inertia of a cylinder is given by

$$I = \left(\frac{d_{outer}^4 - d_{inner}^4}{64}\right)\pi$$

Assuming a constant curvature along the cable length, the curvature can be defined by

$$\kappa = \frac{1}{r} = \frac{2\cdot\theta}{L} \tag{8}$$

where r is the bending radius, θ is the angle at the cable end and L is the cable length.

According to [9], the bending stiffness in the stick regime (no relative sliding between a armour layer and a plastic layers) is found to be more or less the same as for a steel pipe of similar dimensions.

2.6.3 Torsional stiffness

The torsional stiffness is defined as the rate of torsion moment required per torsion angle normalized over the cable length, and is calculated as

$$k_{torsion} = \frac{\Delta M_{torsion}}{\Delta \theta_{torsion}} \tag{9}$$

where $M_{torsion}$ is the moment applied and $\theta_{torsion}$ is the resulting torsion angle per cable length in [rad/m].

3 Model set up

The geometry of the models studied in this thesis are created in ANSYS-Design Modeler 14.5.7, while the set up of the analyses are done in ANSYS Workbench 14.5.7. To solve the analyses, LS-DYNA is used.

For different models are developed and analysed:

- **Model 1:** A simple flexible cable of structural steel
- **Model 2:** A friction element
- **Model 3** A flexible cable with one tendon
- **Model 4** A flexible cable with two armour layers

Each model will be presented more carefully in the next sections, which implies their geometric structure, mesh, contact definitions and their loading and boundary conditions.

3.1 Unit system and material properties

The unit system and material properties used throughout all the analyses are presented in the tables below.

Property	**Unit**
Time	s
Distance	mm
Mass	kg
Velocity	mm/s
Acceleration	mm/s^2
Force	N
Moment	Nmm
Pressure	Mpa

Table 1: Unit system used throughout the analyses

Property	**Unit**	**Structural steel**
Young's Modulus	GPa	200
Poisson's Ratio	-	0,3
Density	kg/m^3	7850

Table 2: Material properties of structural steel

Property	**Unit**	**Polyethylene**
Young's Modulus	GPa	1,1
Poisson's Ratio	-	0,42
Density	kg/m^3	950

Table 3: Material properties of Polyethylene

3.2 Geometry

The geometry of the four different models mentioned initially, will be presented in this sub section. The stiffness behavior is set to flexible for all parts except for additional elements in terms of two fixed rigid plates situated at the end of each cable.

Model 1 and 2 are only assigned to the material of structural steel. Model 3 and 4 on the other hand, are assigned to both structural steel and polyethylene.

3.2.1 Geometry - Model 1

This model is of a flexible cable, and is based on a cylinder of structural steel with geometrical properties tabulated in table 4. The aim of developing this model is to analyse whether or not a simple flexible cable behaves according to theory, hence to see how accurate ANSYS LS-Dyna is when handling such a simple model.

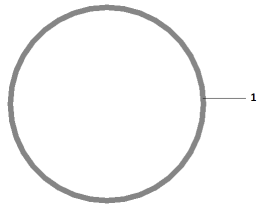

Figure 8: Cross-section of model 1

ID	Part	r_i [mm]	r_o [mm]	t [mm]
1	Cylinder	85	90	5

Table 4: Dimensions of model 1

The geometry is modeled with three different cable lengths (L_i; $i = 1, 2, 3$) where $L_1 = 2000$ mm, $L_2 = 4000$ mm and $L_3 = 6000$ mm for comparison purposes.

3.2.2 Geometry - Model 2

As mentioned in section 1.2, the reason why this model is developed and analysed is to see how well ANSYS LD-Dyna handles a simple case of frictional stick-slip. Hence, the aim is to see if a box starts to slide over a fixed surface when subjected to a force. The criteria for sliding is given to be

$$P_z \cdot \mu \geq P_y \tag{10}$$

The friction element model consists of a box (green) placed on a smooth surface (brown). The geometry of the model is shown in the figure below, followed by a table of its dimensions

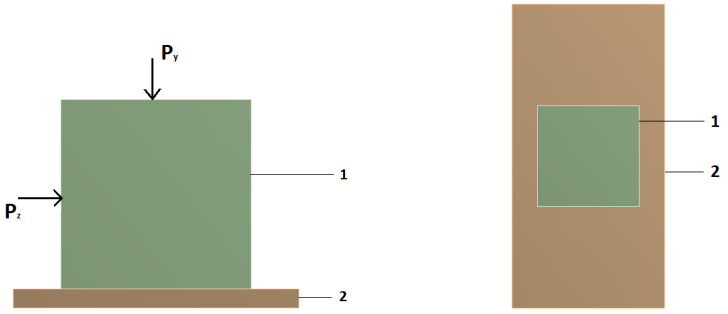

(a) Front (b) Top

ID	Part	Hight [mm]	Width [mm]	Depth [mm]
1	Box	100	100	100
2	Plate	10	150	300

Table 5: Dimensions of parts in model 2

3.2.3 Geometry - Model 3

Originally the tensile armour layers in a umbilical cable consists of helically wound tendons to sustain tensile loads and internal pressure. The layers are normally counter wound in pairs (ref figure 1), and the lay angle is typically between 20 and 55 dregrees [5].

The model consists of two simple flexible cylinders (one inner and one outer) acting as coats, and one tendon wound around the inner coat. The coats are assigned to the material of polyethylene while the tendon is of structural steel.

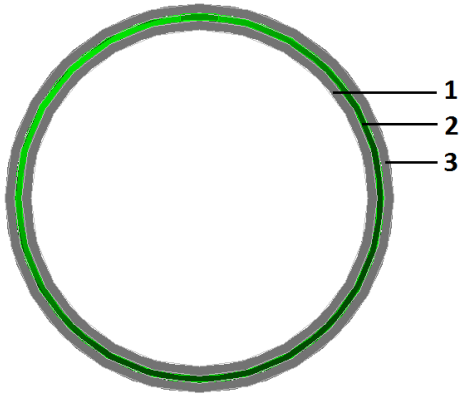

(a) Cross section of model 3

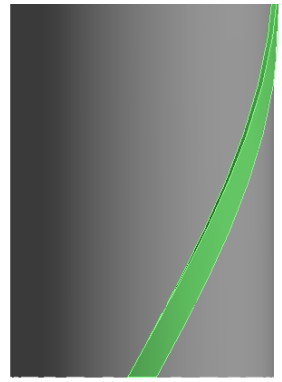

(b) Tendon wound around the inner coating

ID	Part	r_i [mm]	r_o [mm]	t [mm]
1	Inner coat	$80,00$	$84,50$	$4,5$
2	Tendon	$84,65$	$87,85$	$3,2$
3	Outer coat	$88,00$	$92,50$	$4,5$

Table 6: Dimensions of parts in model 3

For practical purposes there are modeled small gaps of 0,2 mm between the inner coat and the tendon, and between the tendon and the outer coat.

When modeling helically wound tendons one should take in to account at least two pitch lengths (L_p), where a pitch length is defined by:

$$L_p = \frac{2\pi \cdot r_m}{\tan \alpha}, \qquad \text{where} \quad r_m = \frac{r_o + r_i}{2} \tag{11}$$

Based on cable length L_1 from model 1, and assuming the requirement of two pich lengths, the lay angle is $\alpha = 28,45°$ which is a likely presumption.

The cross section design of the tendon is shown in figure 11, where $R71$ and $R70$ are the inner and outer radius respectively (ref table 6), and the angle $A73$ is 12°.

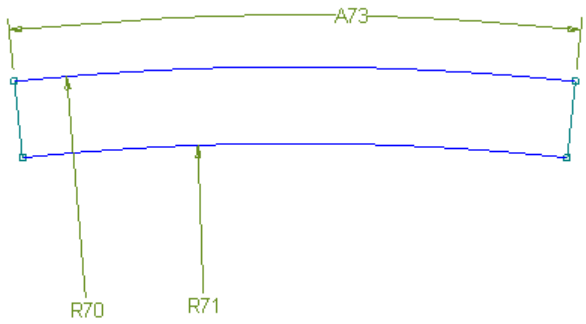

Figure 11: Armour thread design

3.2.4 Geometry - Model 4

What differs this model from model 3 is that the initiated armour layer in model 3 now is completed with 30 tendons wound around the inner cylinder. This model has also expanded to include another armour layers outside the first one, where the inner layer is wound with a "left“ helical lay direction and the outer layer with a "right“ helical lay direction.

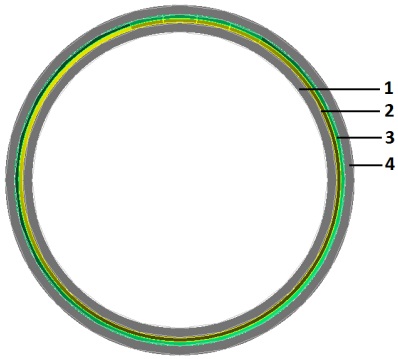

(a) Cross section of model 4

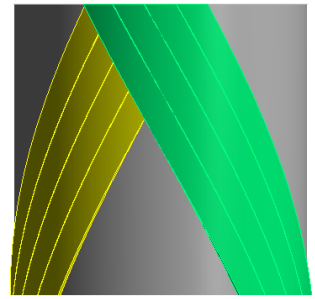

(b) Inner and outer armour layers

The tendons has the same cross section design as in model 3, but to make sure to include a small gap between all the tendons, the angle A73 in figure 11 is reduced to 11,6°.

ID	Part	r_i [mm]	r_o [mm]	t [mm]
1	Inner coat	80,00	84,50	4,5
2	Armour layer 1	84,65	87,85	3,2
3	Armour layer 2	88,00	92,50	4,5
4	Outer coat	88,00	92,50	4,5

Table 7: Dimensions of parts in model 4

3.3 Coordinate systems

The global coordinate system that is shown in figure 13 is representative for model 1, 3 and 4.

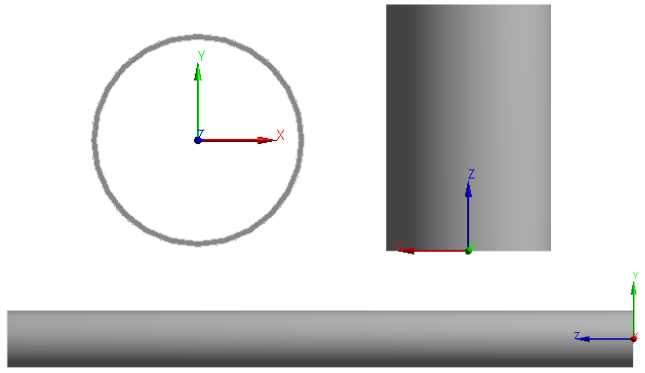

Figure 13: Global coordinate system

The rigid plates connected to the cable ends are each assigned with its own local coordinate system, which is shown in figure 14

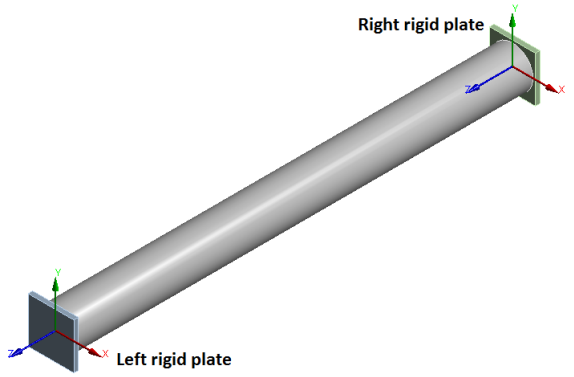

Figure 14: Local coordinate system of rigid plates

3.4 Mesh

There are certain requirements to take in to account when meshing explicit applications. Consideration should be given to the number of elements in the model and the quality of the mesh to give larger resulting time steps and therefore more efficient simulations [2].

Since the cable geometry in model 1, 3 and 4, and the tendon geometry in model 3 and 4 is uniform with a single source- and target face, the mesh method is set to sweep to generate pure hex meshes. This is preferred when handling a solid body model as in this case. A hex mesh is based on reduced integration for first order elements which means that there is only one integration point per element. As mentioned in section 2.3, such elements are the most efficient and they minimize the computational expenses of element calculations as well as they sometimes are more accurate for slower transients [3].

Before the models are swept, the size of the mesh is controlled by the cross section of the cable through edge sizing, where a number of divisions in the axial direction is set. The amount of divisions are increased in model 3 and 4 to make sure the tendons wound well around the inner coat. The sweep of the tendon(s) and the coats are carefully applied with equal amount of divisions to make sure the nodes between the two bodies initially lines up.This is done for better control of tracking any relative displacement and/or velocity later on. More details of the mesh controls is now presented in the following sub sections.

3.4.1 Mesh - Model 1

ID/Part	Size Control	Value
1	Circumfurence divisions	40
1	Sweep direction spacing	35 divisions/meter
1	Radial mapped face sizing	2
Rigid plates	Body sizing	75 mm

Table 8: Mesh controls for model 1

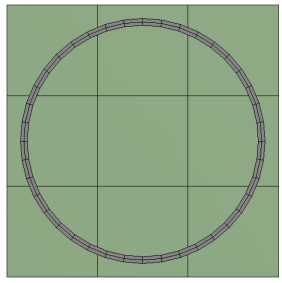

(a) Mesh of cross section

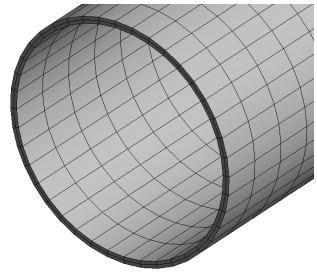

(b) Mesh of cable end

(c) Mesh of entire body

Figure 15: Mesh of model 1

	2000 mm	4000 mm	6000 mm
Numbers of elements	5618	11218	16818
Number of nodes	8584	16984	25384

Table 9: Number of elements and nodes in model 1

3.4.2 Mesh - Model 2

This model is only meshed with body size control of 5 mm on both the box and the plate. To capture the behavior of sliding as good as possible, it is important to make sure that the nodes between the box and the plate initially lines up. This can be seen to the left in figure 16

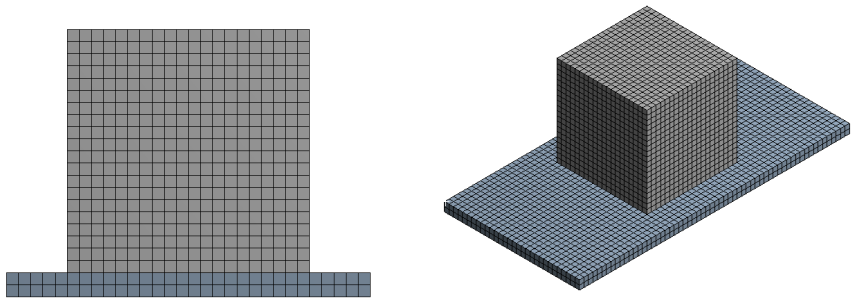

Figure 16: Mesh of model 2

	Model 2
Numbers of elements	11600
Number of nodes	14934

Table 10: Number of elements and nodes in model 2

3.4.3 Mesh - Model 3

ID/Part	Size Control	Value
2	Circumfurence divisions	3
1, 3	Circumfurence divisions	60
1, 2, 3	Sweep direction spacing	50 divisions/meter
1, 3	Radial face sizing	2
Rigid plates	Body sizing	15 mm

Table 11: Mesh controls for model 1

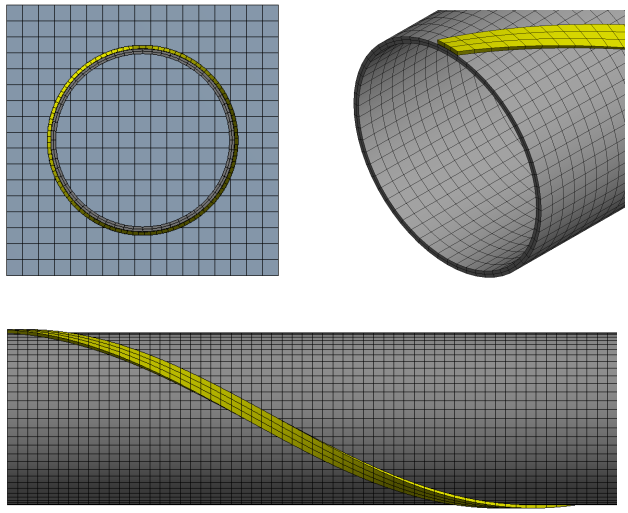

(a) Mesh of tendon wound about the cylinder

Figure 17: Mesh of model 3

	Model 3
Numbers of elements	98356
Number of nodes	149512

Table 12: Number of elements and nodes in model 3

3.4.4 Mesh - Model 4

ID/Part	Size Control	Value
2, 3	Circumfurence divisions	3
1, 4	Circumfurence divisions	60
1, 2, 3, 4	Sweep direction spacing	50 divisions/meter
1, 4	Radial face sizing	2
Rigid plates	Automatic	-

Table 13: Mesh controls for model 4

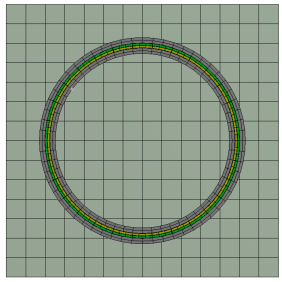

(a) Mesch of cross section

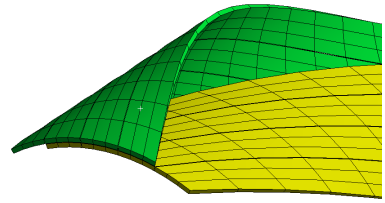

(b) Mesh of armour layers

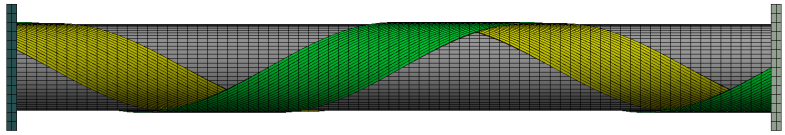

(c) Mesh of armour layers wound about the inner coat

Figure 18: Mesh of model 4

	1000 mm	1500 mm	2000 mm
Numbers of elements	22156	32284	42288
Number of nodes	44784	65190	85516

Table 14: Number of elements and nodes in model 4

3.5 Contact definitions

The contact definition between parts in each model will be presented in this section. It will appear that that the contact between the rigid plates and the cable ends are set to bonded (model 1, 3 and 4). This contact may give unrealistically stiff constraints at the cable sides, which is one of the reasons for why different cable lengths are analysed.

3.5.1 Contact definitions - Model 1

Manual contact regions are created in this model. A bonded contact is set between the cylinder ends and the rigid plates, with a maximum offset of 0,0001 mm and a trim tolerance of 5,1488 mm. This means that the contacts created are not breakable.

3.5.2 Contact definitions - Model 2

Manual contact regions are created. Between the box and the plate the contact is set to frictional with a friction coefficient of $\mu = 0,2$. There is no distinction between static or dynamic friction, which means that the friction coefficient is 0,2 regardless of whether the two bodies are sliding or sticking to each other.

3.5.3 Contact definitions - Model 3

Manual contact regions are created, and an overview of how the different bodies are connected to each other is presented in table 15

	Rigid plates	**Inner/Outer coating**	**Tendon**
Rigid plates	-	Bonded	Bonded
Inner/Outer coating	Bonded	-	$\mu = 0,2$
Tendon	Bonded	$\mu = 0,2$	-

Table 15: Interaction between parts in model 3

The frictional contacts have symmetrical behaviour as well as a trim tolerance of 3 mm.

3.5.4 Contact definitions - Model 4

Manual contact regions are created, and an overview of how the different bodies are connected to each other is presented in table 16.

ID	**Rigid plates**	**1**	**2**	**3**	**4**
Rigid plates	-	Bonded	Bonded	Bonded	Bonded
1	Bonded	-	$\mu = 0,2$	-	-
2	Bonded	$\mu = 0,2$	-	$\mu = 0,2$	-
3	Bonded	-	$\mu = 0,2$	-	$\mu = 0,2$
4	Bonded	-	-	$\mu = 0,2$	-

Table 16: Interaction between parts in model 4

Also, a manually body interaction contact is created to make sure that all the tendons within each layer are able to slide relative to each other. Similar to the other frictional contacts created, the friction coefficient is set to $\mu = 0,2$, and is constant throughout the analyses.

3.6 Loading and boundary conditions

The behaviour of the cables are controlled by movement of the rigid plates connected to the cable ends. By applying forces to these plates it is possible to track the resulting reaction forces/moments or displacements which again make it possible to extract the cable stiffness response.

3.6.1 Loading and boundary conditions - Model 1

Axial stiffness: To find the axial stiffness, model 1 is subjected to an axial force of 50 kN. The rigid body constraint definitions of both the left- and right rigid plate are set to fixed, except for the Z-component of the left rigid plate that is set to free to allow deformation in this direction.

The force of 50 kN is applied in a linear load step, which is illustrated in figure 19.

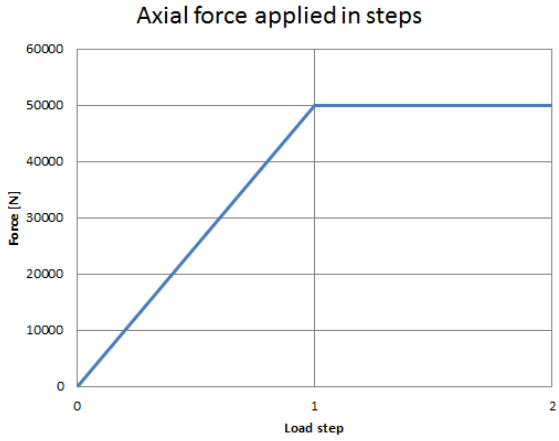

Figure 19: Load step application of axial load - Model 1

During the second load step, the force is held constant, hence this load step is named the constant load step. The annotation of “constant load step” will also be used later on in relation to the other analyses.

Bending Stiffness: To find the bending stiffness, both rigid plates are rotated about the x-axis. The applied angle vary with the cable length which means that the curvature is kept constant throughout all the bending analyses. The table below shows the magnitude of the rigid body rotations of the different cable lengths:

	2000 mm	**4000 mm**	**6000 mm**
$\Delta\theta$	5°	10°	15°

The load step application of the curvature applied is illustrated in figure **??**

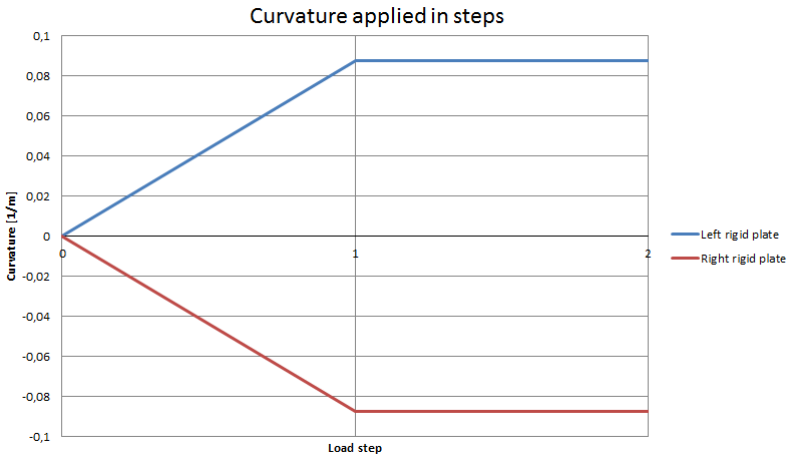

Figure 20: Load step application of curvature - Model 1

where load step 1 is linearly ramped and load step 2 is held constant. The following boundary conditions are applicable during this analysis:

	X Comp.	**Y Comp.**	**Z Comp.**
Left rigid plate	Fixed	Fixed	Fixed
Right rigid plate	Fixed	Fixed	Fixed
	Rot. X	**Rot. Y**	**Rot. Z**
Left rigid plate	Free	Fixed	Fixed
Right rigid plate	Free	Fixed	Fixed

Table 17: Rigid body constraint during bending - Model 1

Torsional stiffness: To find the torsional stiffness, a rigid body rotation is applied to the left rigid plate about the Z-axis with the following load step application:

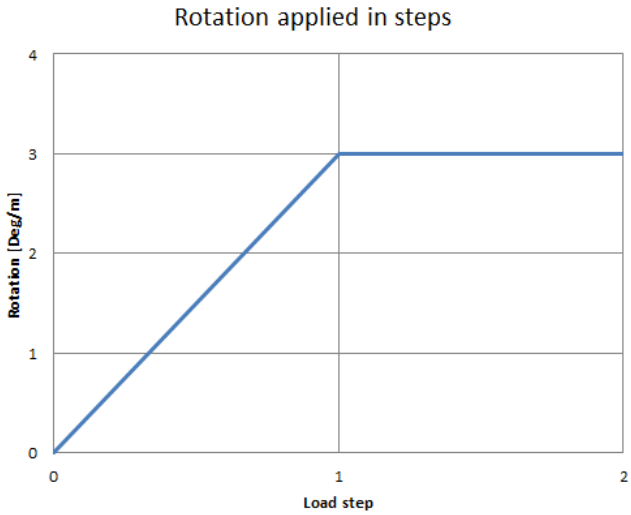

Figure 21: Step application of torsion - Model 1

The corresponding boundary conditions are:

	X Comp.	**Y Comp.**	**Z Comp.**
Left rigid plate	Fixed	Fixed	Fixed
Right rigid plate	Fixed	Fixed	Fixed
	Rot. X	**Rot. Y**	**Rot. Z**
Left rigid plate	Fixed	Fixed	Fixed
Right rigid plate	Fixed	Fixed	Free

Table 18: Rigid body constraint during torsion - Model 1

3.6.2 Loading and boundary conditions - Model 2

This model is subjected to pressure at the top of the box (in negative y-direction) and at one of the sides of the box (in z-direction) to provoke sliding. The load steps of the two pressure forces are applied in the following way:

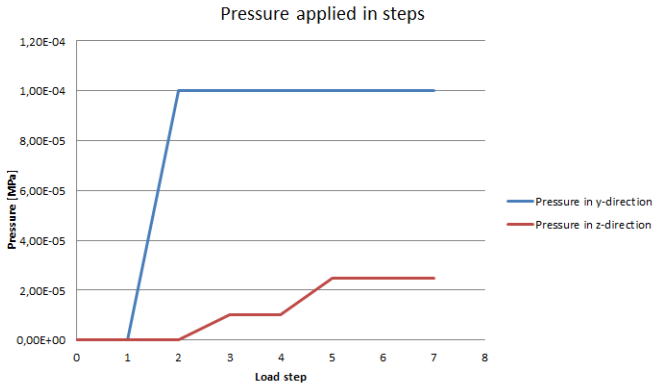

Figure 22: Step application of loading - Model 2

The pressure P_z differs from the pressure P_y by the magnitude of $\mu = 0,2$, and P_z is increasing during the load path until it reaches a value greater that P_y. Theoretically sliding should then occur at load step 5.

The flexible plate is set to be fixed at all time, to allow the box to slide on its top surface.

3.6.3 Loading and boundary conditions - Model 3

Model 3 is only analysed during bending, and the load step application is shown in figure 23. Remark that the cable is subjected to an initial pre-tension of 5kN to make sure that the tendon is in stick with the coats before the rigid body rotation is applied.

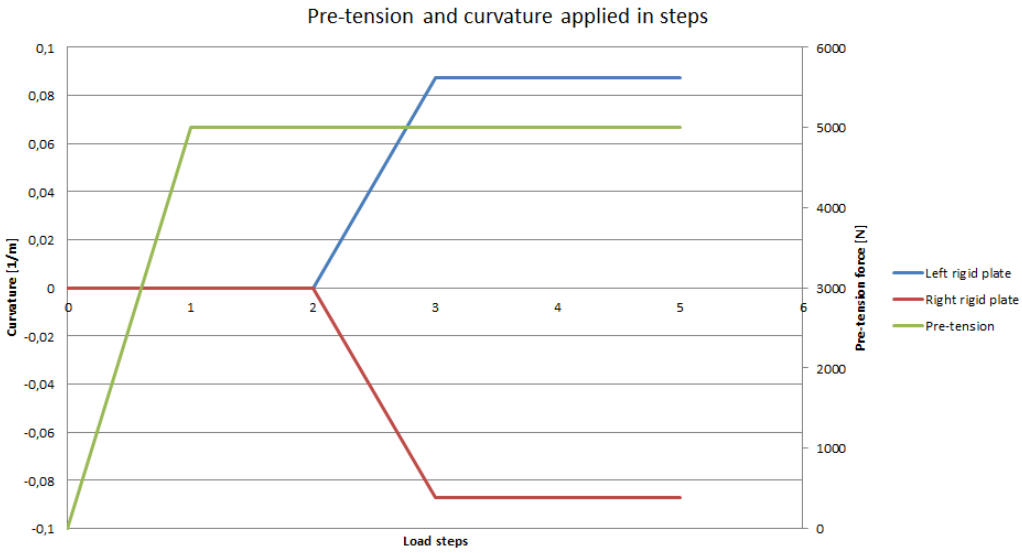

Figure 23: Load step application of pre-tension and bending - Model 3

The boundary conditions applied to this model are:

	X Comp.	Y Comp.	Z Comp.
Left rigid plate	Fixed	Fixed	Free
Right rigid plate	Fixed	Fixed	Fixed
	Rot. X	**Rot. Y**	**Rot. Z**
Left rigid plate	Free	Fixed	Fixed
Right rigid plate	Free	Fixed	Fixed

Table 19: Rigid body constraints during bending - Model 3

3.6.4 Loading and boundary conditions - Model 4

Below, the load step applications of bending and torsion is presented, as well as the boundary conditions applied respectively. Notice that this model is also initially subjected to a pre-tensional load og 5 kN.

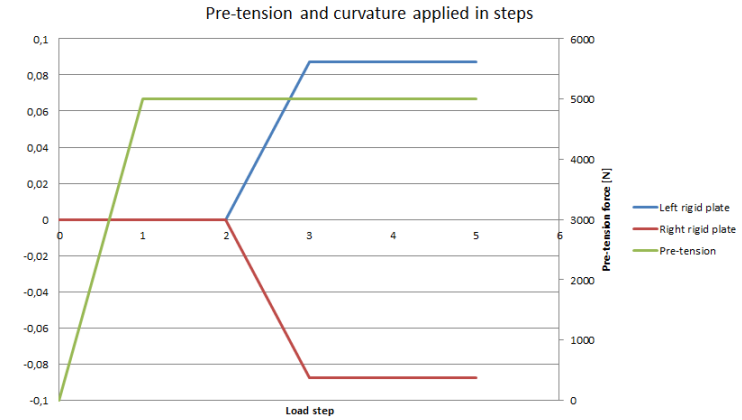

Figure 24: Load step application of pre-tension and bending - Model 4

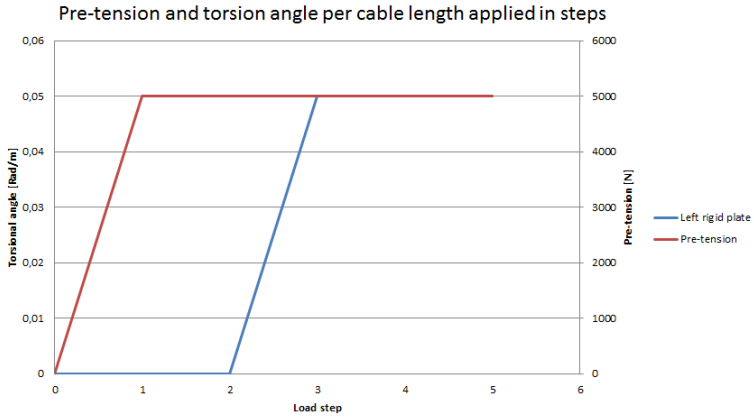

Figure 25: Load step application of pre-tension and torsion - Model 4

The magnitude of the rigid body rotations of the different cable lengths analysed are:

	1000 mm	**2000 mm**	**3000 mm**
$\Delta\theta$	2,5°	5°	7,5°

and the boundary conditions applied are

	X Comp.	**Y Comp.**	**Z Comp.**
Left rigid plate	Fixed	Fixed	Free
Right rigid plate	Fixed	Fixed	Fixed
	Rot. X	**Rot. Y**	**Rot. Z**
Left rigid plate	Free	Fixed	Fixed
Right rigid plate	Free	Fixed	Fixed

Table 20: Rigid body constraints during bending - Model 4

	X Comp.	**Y Comp.**	**Z Comp.**
Left rigid plate	Fixed	Fixed	Free
Right rigid plate	Fixed	Fixed	Fixed
	Rot. X	**Rot. Y**	**Rot. Z**
Left rigid plate	Fixed	Fixed	Free
Right rigid plate	Fixed	Fixed	Fixed

Table 21: Rigid body constraints during torsion - Model 4

4 Results

In this section, the results from all the analyses will be presented. A more detailed discussion of the results will follow in section.

All the analyses are presented with system energy plots to validate the quasi-static solution. 4.6.

4.1 Results - Model 1

This model is not subjected to pre-tension at this stage.

Three different analyses, axial-, bending and torsional stiffness analyses, have been run, and each analysis is run with three different cable lengths, $L = 2000$ mm, $L = 4000$ mm and $L = 6000$ mm.

4.1.1 Axial stiffness

The results from the axial stiffness analysis are normalized over the cable length, and found from average values of the axial deformation over the constant load step.

Analysis	**2000 mm**	**4000 mm**	**6000 mm**
Axial deformation [mm]	0,18269	0,36621	0,54893
Axial stiffness [MN]	547,376	542,846	546,518

Table 22: Results from the axial stiffness analyses - Model 1

Because of initial problems with high hourglass energy, the axial stiffness analyses have been run with the hourglass control setting; Flanagan-Belytschko Stiffness, with an default hourglass coefficient of 0,03.

The axial deformation histories from the three different analyses are shown in the figures below, where the constant load step presented in section 3.6.1 is situated between $0{,}05 < t < 0{,}1$. Further the system energies for all the bodies in the respective analyses are presented, including the hourglass control setting.

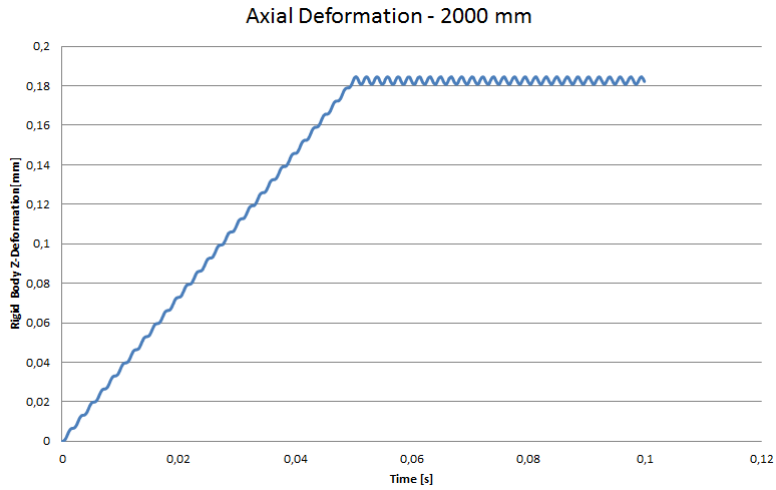

Figure 26: Axial deformation of left rigid plate - 2000 mm - Model 1

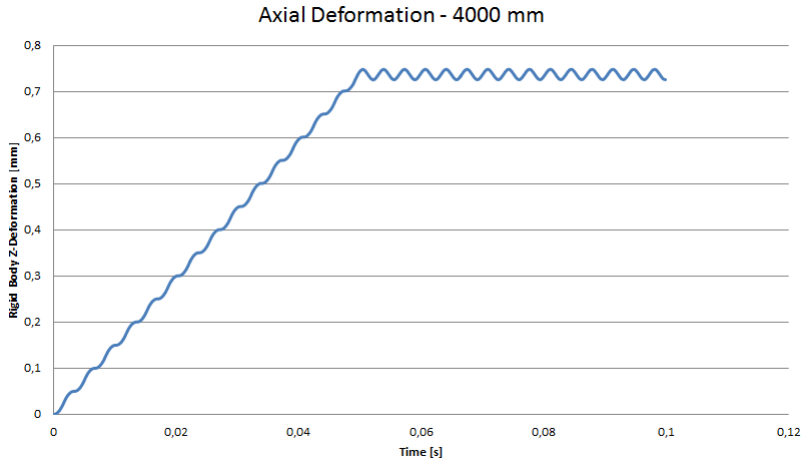

Figure 27: Axial deformation of left rigid plate - 4000 mm - Model 1

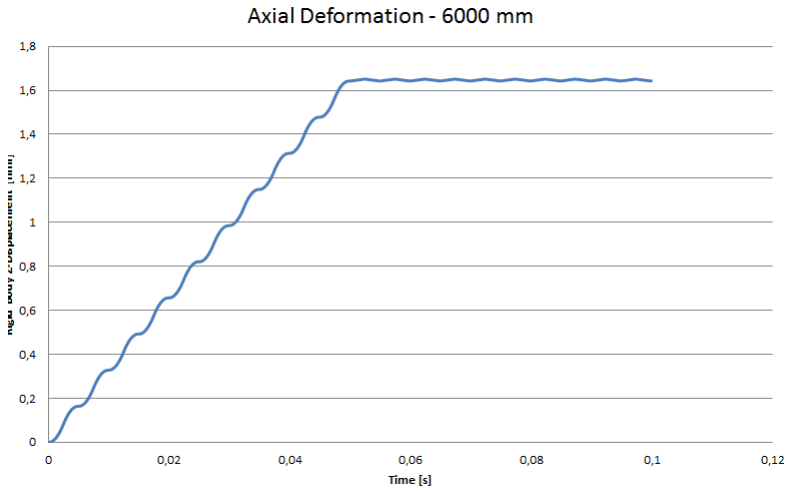

Figure 28: Axial deformation of left rigid plate - 6000 mm - Model 1

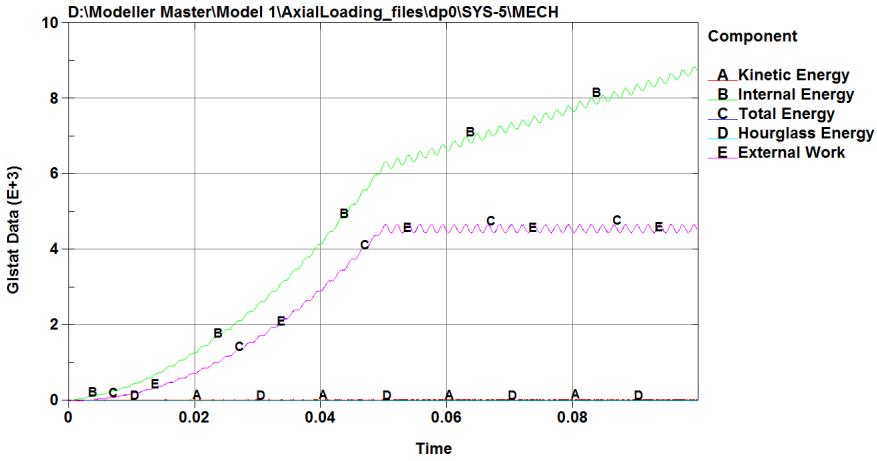

Figure 29: System energies, all bodies - 2000 mm - Model 1

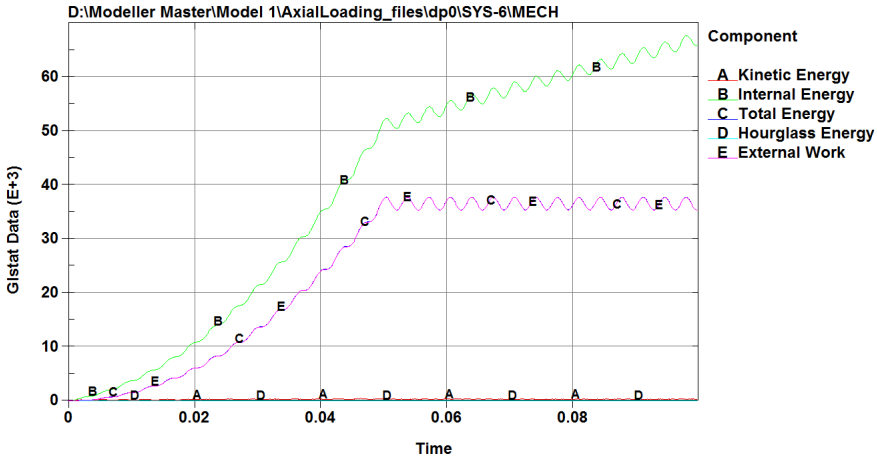

Figure 30: System energies, all bodies - 4000 mm - Model 1

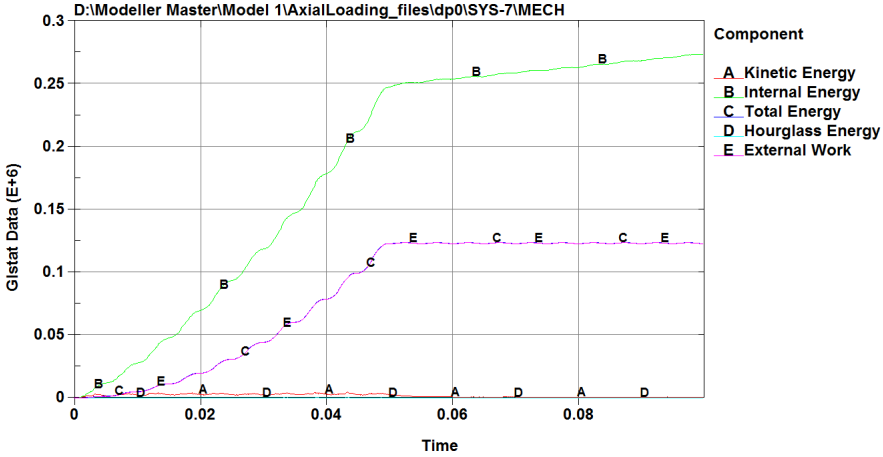

Figure 31: System energies, all bodies - 6000 mm - Model 1

4.1.2 Bending stiffness

The theoretical bending stiffness of the geometry of model 1 is given by

$$k_{bending} = EI = 2 \cdot 10^{11} \left(\frac{d_o^4 - d_i^4}{64} \right) \pi = 2{,}106 \ MNm^2 \tag{12}$$

If extracting the bending moment reactions and the corresponding curvatures at each load step (labeled with the sub indices 0, 1 and 2), the following values are found:

Load step/Analysis	**2000 mm**	**4000 mm**	**6000 mm**
κ_0 [1/m]	0	0	0
M_0 [kNm]	0	0	0
κ_1 [1/m]	0,9	0,9	0,9
M_1 [kNm]	173	149,9	149,6
κ_2 [1/m]	0,9	0,9	0,9
M_3 [kNm]	180,8	166,9	183,6

Table 23: Bending moment reactions for the steps in the bending stiffness analyses

The results from the bending stiffness analyses are presented in the table below. Note that the results are found from average values over the respective load regions.

Load step/Analysis	**2000 mm**	**4000 mm**	**6000 mm**
$k_{1,bending}$ [MNm^2]	2,0	2,0	2,095
$k_{2,bending}$ [MNm^2]	2,07	1,91	2,103

Table 24: Results from the bending stiffness ananlyses - Model 1

The results from both load step 1 (ramped load region) and load step 2 (constant load region) are close to equal the theoretical value of the bending stiffness. Hence it does not make to much of a difference from which load step the results are extracted from.

Further, the y-directional deformation-, x-moment reaction and the system energies for all the three cable lengths, is presented.

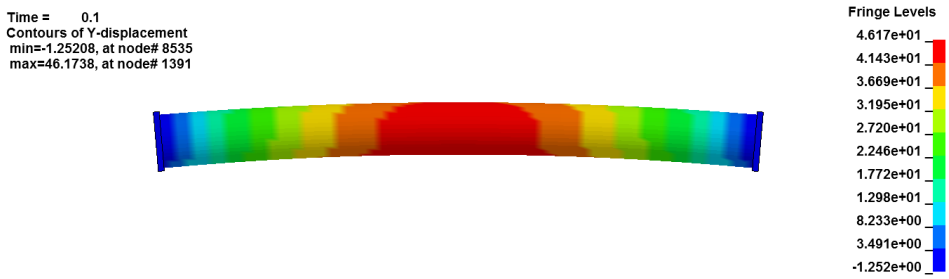

Figure 32: Y-Directional deformation at end time - 2000 mm - Model 1

Figure 33: Y-Directional deformation at end time - 4000 mm - Model 1

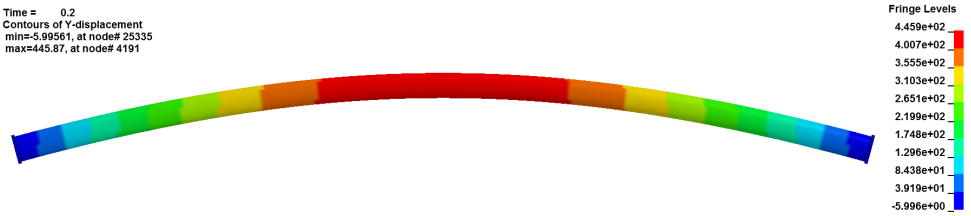

Figure 34: Y-Directional deformation at end time - 6000 mm - Model 1

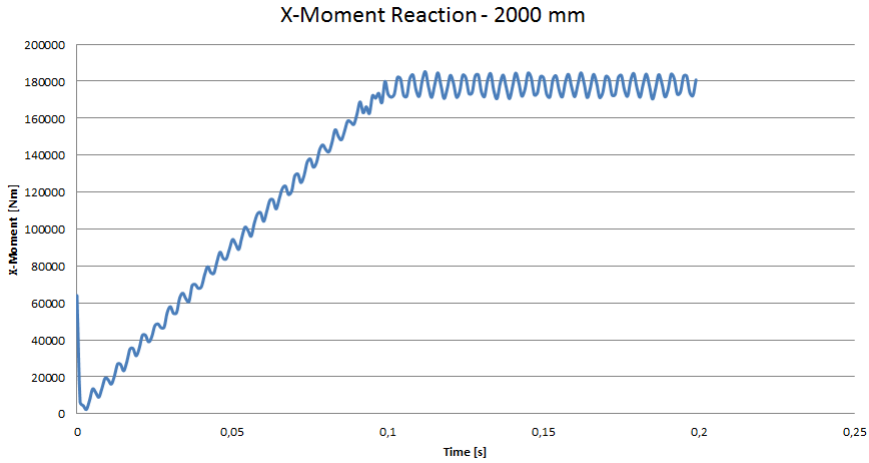

Figure 35: X-Moment reactions at left rigid plate - 1000 mm - Model 1

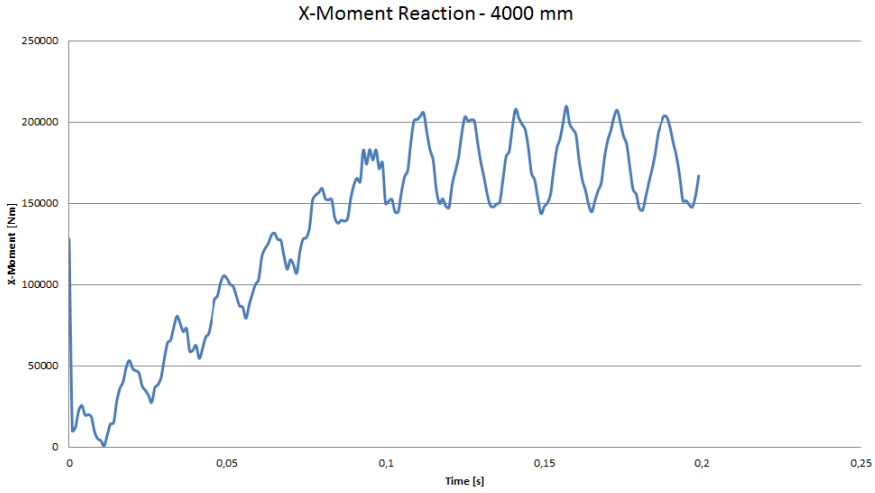

Figure 36: X-Moment reactions at left rigid plate - 4000 mm - Model 1

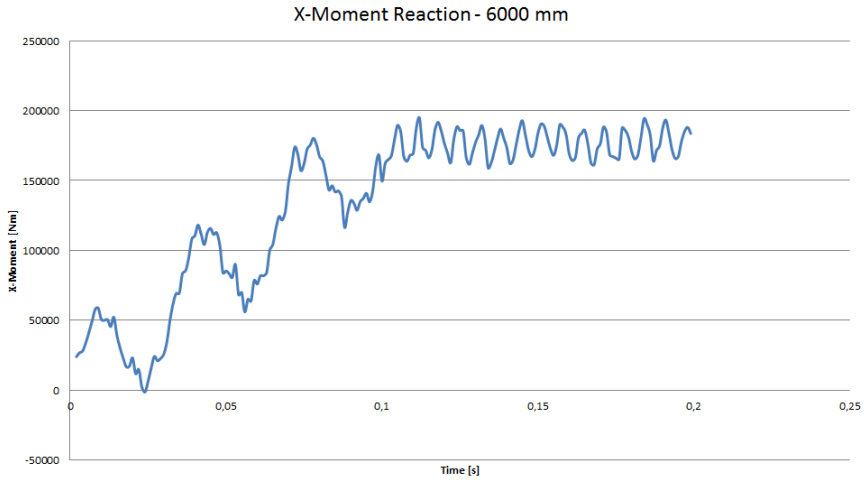

Figure 37: X-Moment reactions at left rigid plate - 6000 mm - Model 1

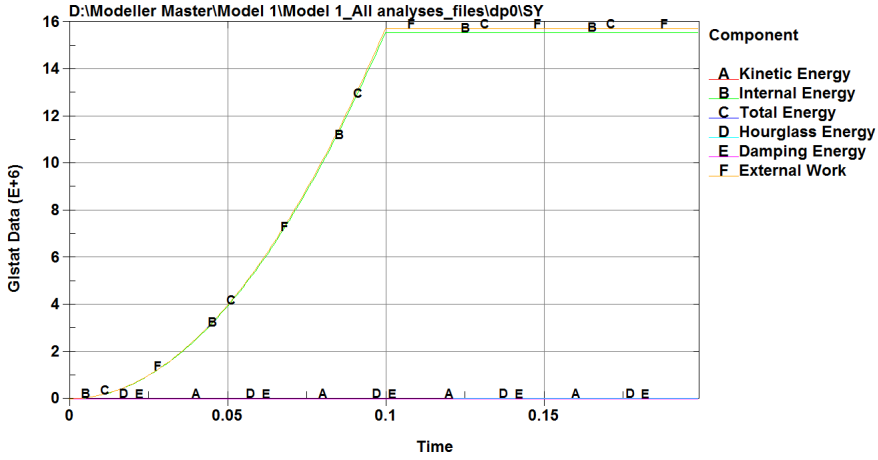

Figure 38: System energies, all bodies - 2000 mm - Model 1

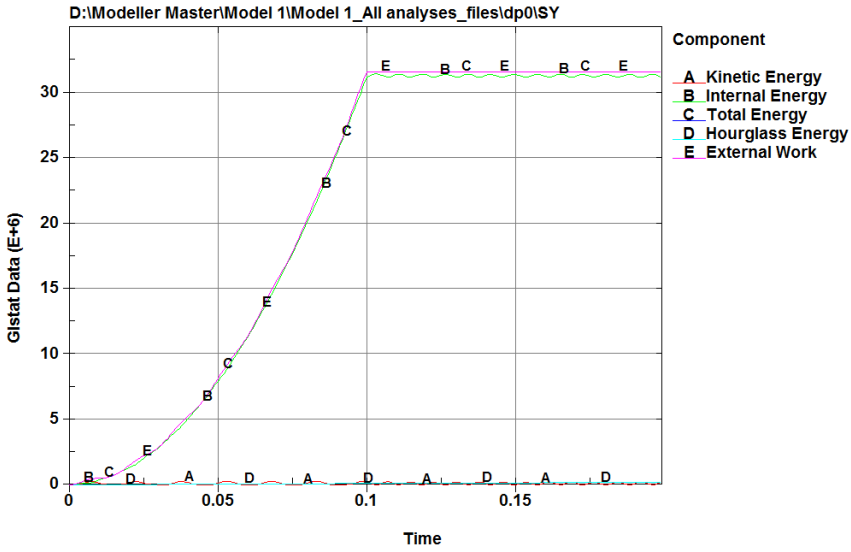

Figure 39: System energies, all bodies - 4000 mm - Model 1

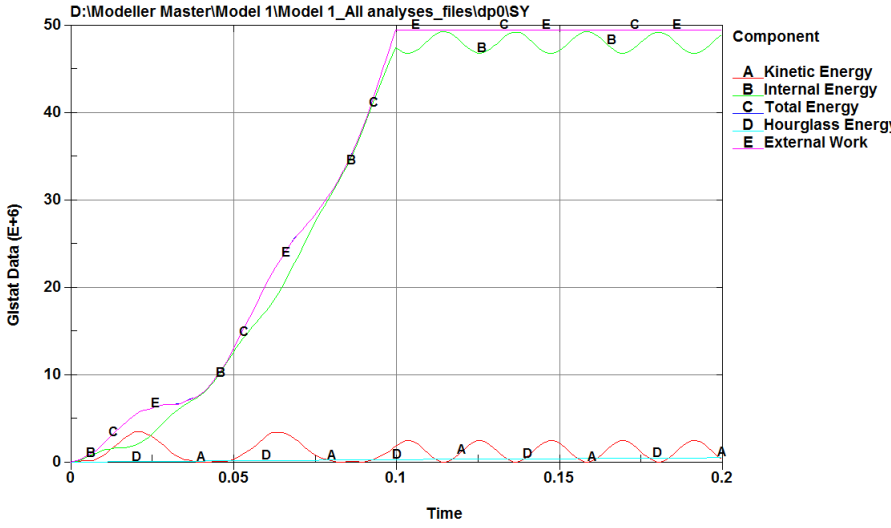

Figure 40: System energies, all bodies - 6000 mm - Model 1

4.1.3 Torsional stiffness

Based on the applied load steps presented in section 3.6.1, these are the following results from the torsional stiffness analyses:

Analysis	**2000 mm**	**4000 mm**	**6000 mm**
$\Delta\ \theta_{torsion}$ [Rad/m]	0,025	0,0125	0,008
$\Delta\ M_{torsion}$ [kNm]	104,59	104,68	104,64
$k_{torsion}$ [MNm^2]	1,99	1,99	2,02

Table 25: Results from the torsional stiffness analyses - Model 1

The results are found from average values over the constant load region.

It can be seen that the torsional stiffness is approximately the same for the different cable lengths analysed. Figure 41, 42 and 43 shows that all the analyses have constant z-moment in the constant load region (0,1 < t < 0,2 sec), and that the variation in moment reaction (ΔM) in load step 1 is almost the same for all the cable lengths.

Figures 44, 45 and 46 shows the system energies throughout the analyses.

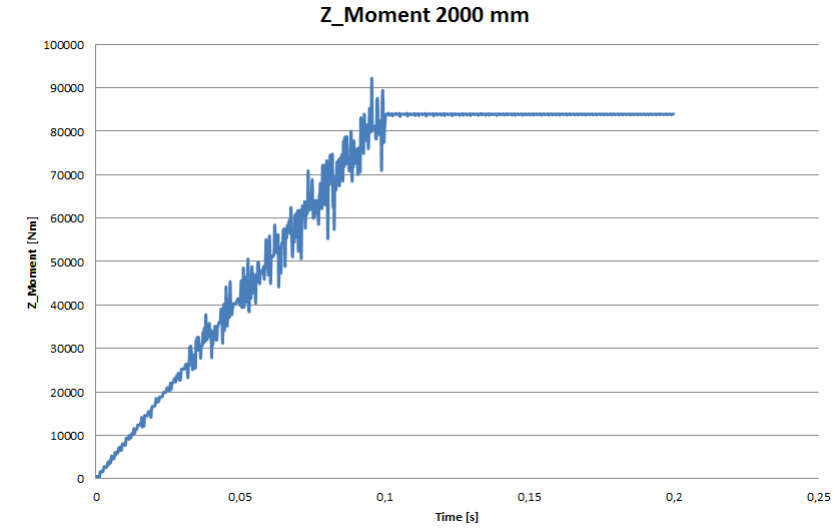

Figure 41: Z-Moment reaction at left rigid plate - 2000 mm

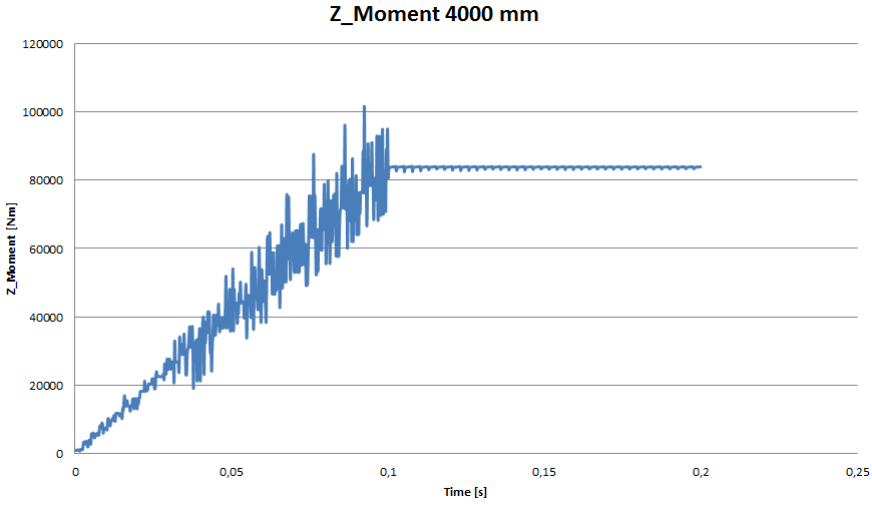

Figure 42: Z-Moment reaction at left rigid plate - 4000 mm

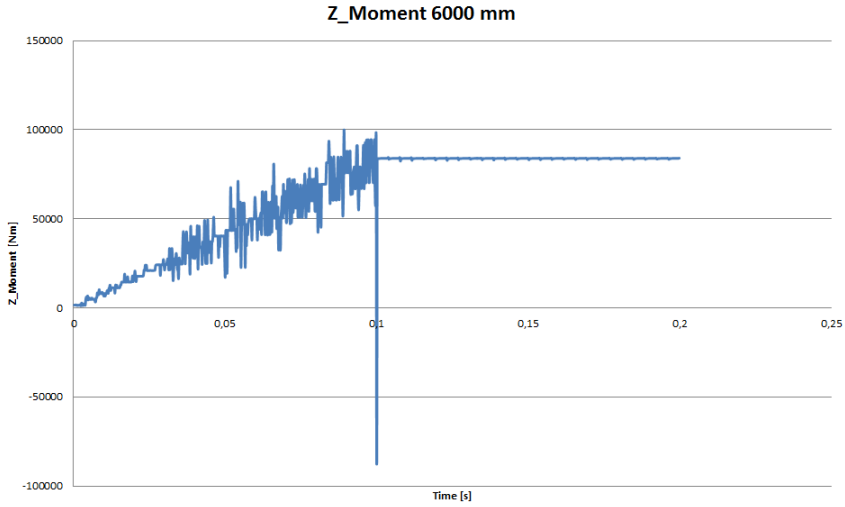

Figure 43: Z-Moment reaction at left rigid plate - 6000 mm

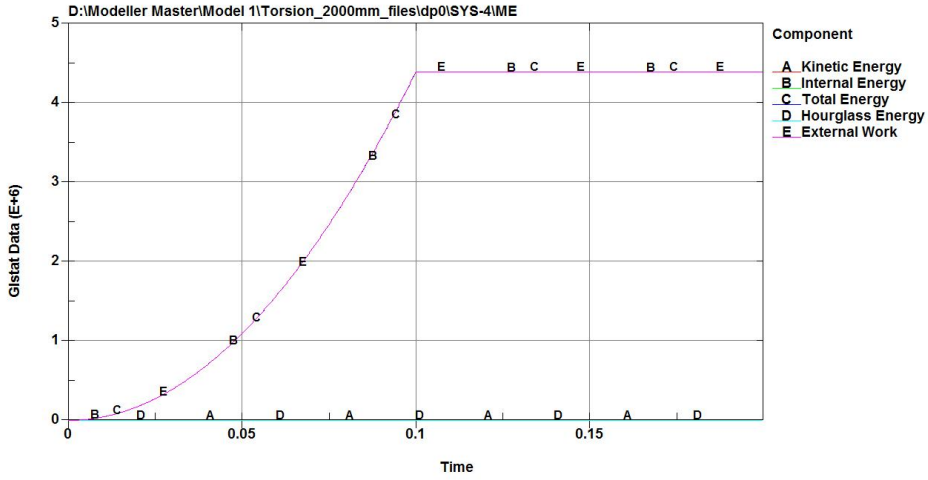

Figure 44: System energies, all bodies - 2000 mm - Model 1

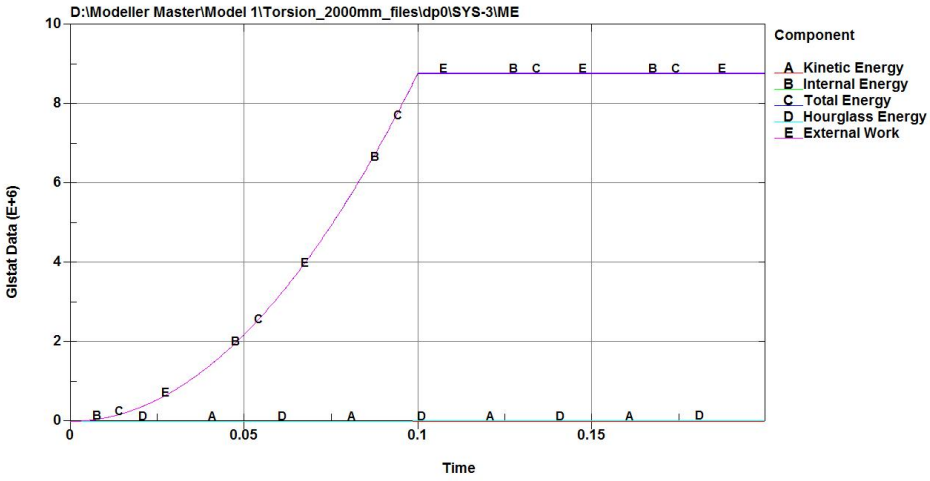

Figure 45: System energies, all bodies - 4000 mm - Model 1

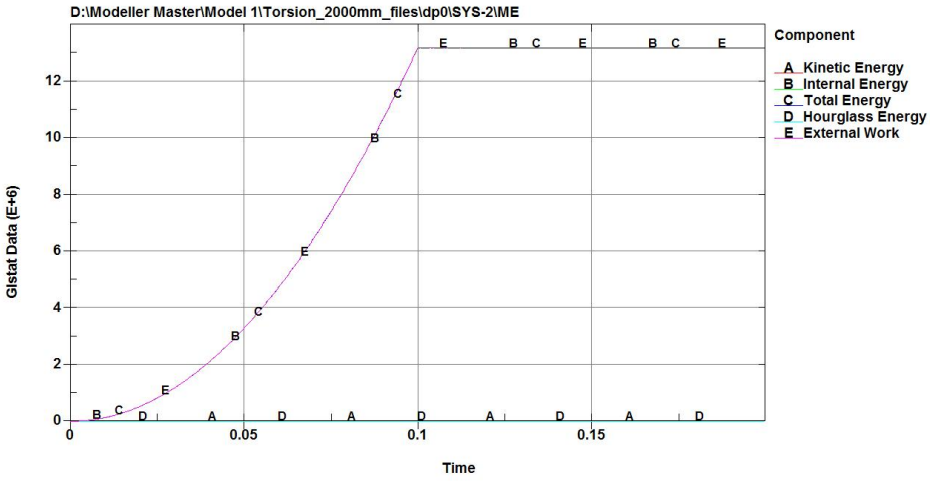

Figure 46: System energies, all bodies - 6000 mm - Model 1

4.2 Results - Model 2

According to figure 47 the assumption presented in section 3.2.2 is satisfied, ie the box starts to slide at load step 5 (indicated by a horizontal line at $t = 0,05$ seconds).

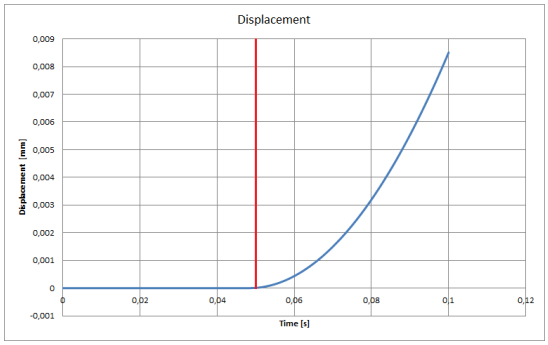

Figure 47: Z-Velocity history of the box

Care has been taken when defining the load steps of the two pressure forces. If the load steps of P_y is not following the exact same load steps as the pressure force P_z, undesirable sequence of events will occur. This is for example that the box will start to slide before or after it should, or it does not slide at all. So, even though P_y is held constant between point 2 and 7 (ref figure 48, point 3, 4, 5 and 6 must be included to follow the path of P_z.

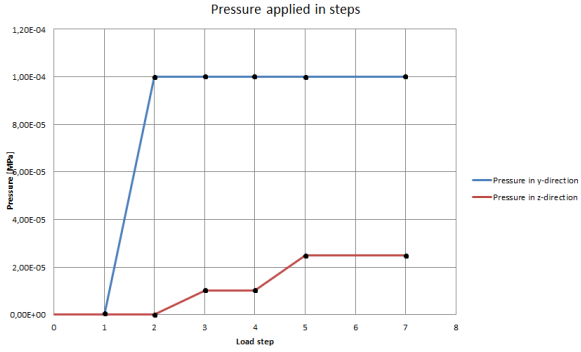

Figure 48: Exact same load step points applied

4.3 Results - Model 3

This model differs from model 1 by the choice of material, as well as the geometry is further developed to have a more complex cross section. Although, it is still rather simple, and the aim of analysing this model with only one tendon, is to capture an optionally stick-slip behavior of the tendon during bending.

Similar to model 1, there was initial detected problems with too high hourglass energy. The hourglass control; Flanagan-Belytschko Stiffness was therefor applied with an hourglass coefficient of 0,03.

Theory in section 2.5 claims that a slip angle of ψ^0 is developed during bending. Therefor, three points of significance are analysed, and a relative interface displacement between the tendon and the inner coat is tracked in all the points.

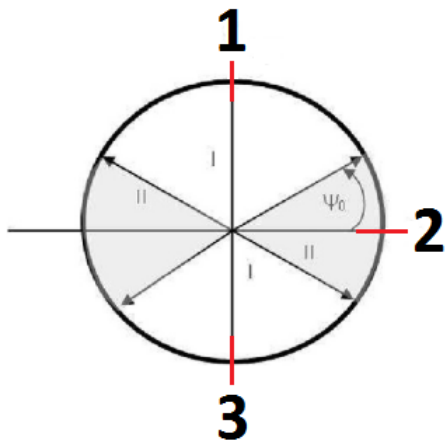

Figure 49: Points analysed - Cross-section view

Figure 50 illustrates how an excerpt from the model is chosen. Because of possible end effects that may give unrealistic or wrong results, the section that is extracted is situated in the middle of the cable.

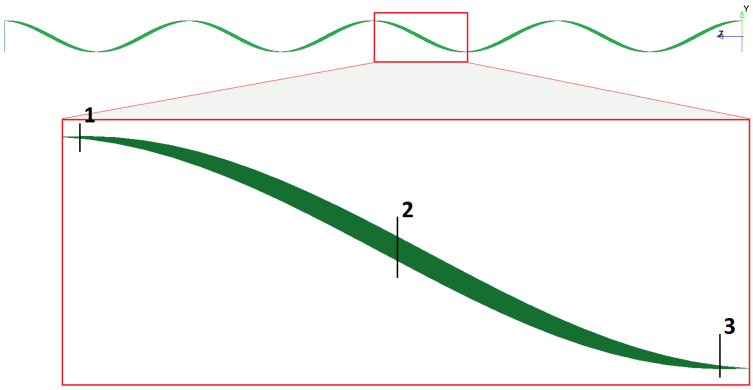

Figure 50: Excerpt from the stick-slip analysis - Model 3

In the bottom part of figure 50 the tendon section excerpted is highlighted, and the three points from figure 49 is marked. The following three graphs shows how the relative interface displacement between the tendon and the inner coat develops in z-direction.

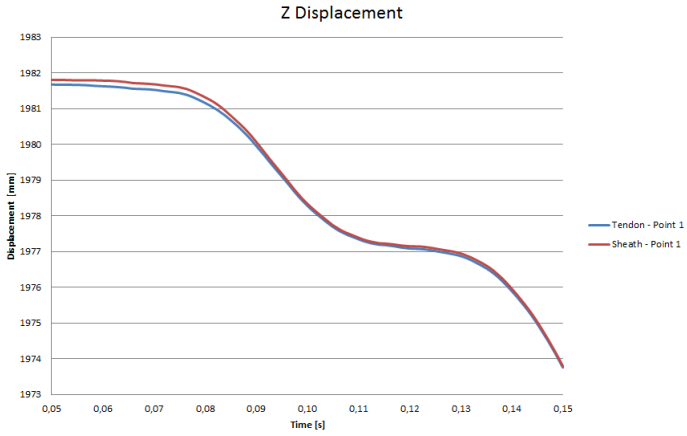

Figure 51: Z-Displacement point 1 - Model 3

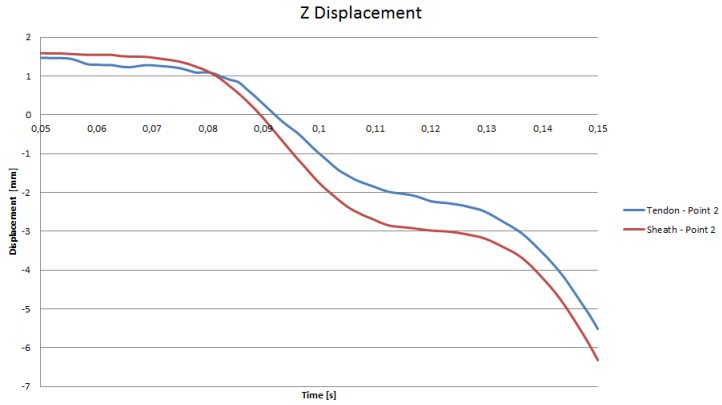

Figure 52: Z-Displacement point 2 - Model 3

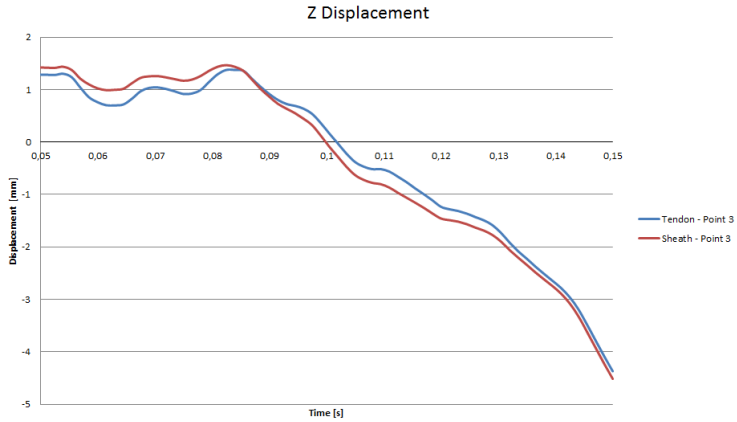

Figure 53: Z-Displacement point 3 - Model 3

As can be seen in figure 52 the relative interface displacement between the tendon and the inner coat differs from each other at the time of approximately 0,08 seconds, that is after 0,03 seconds of bending, and the difference continue to increase during the bending path. This is not the case in point 1 and 3, which implies that the tendon actually slips in the assumed region.

In addition to the change in relative displacement, the plot in figure 54 shows how the yz-stress of point 2 clearly differs from the yz-stress in the two other point during bending (0,05 < t < 0,15 seconds)

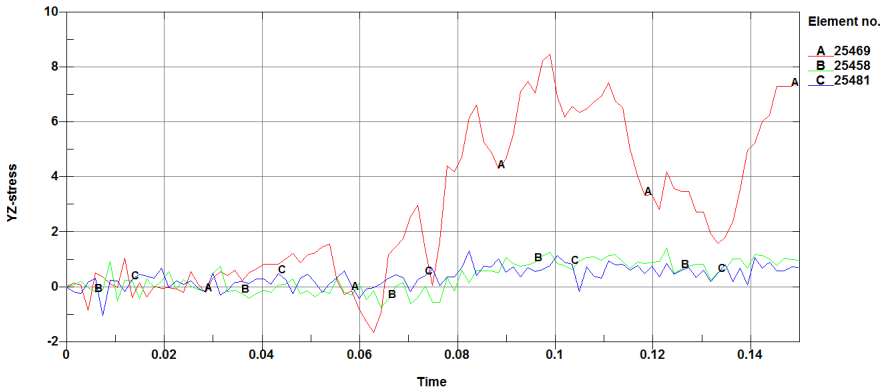

Figure 54: YZ-Stress of tendon- Model 3

Here A25469 = Point 2, B25458 = Point 1 and C25481 = Point 3.

4.4 Results - Model 4

4.4.1 Axial stiffness

The axial stiffness for this model is found in the same way as with model 1, and the results presented in table 26 are average values from the constant load step of the pre-tension applied.

Analysis	1000 mm	2000 mm	3000 mm
Axial deformation [mm]	0,5317	1,1785	1,7651
Axial stiffness [MN]	9,41	8,49	8,49

Table 26: Results from the axial stiffness analyses - Model 4

The axial deformation histories from the three different analyses are shown in the figures below. System energies for all the bodies are presented with the bending- and torsional stiffness analyses, as the pre-tension load is a part of these analyses.

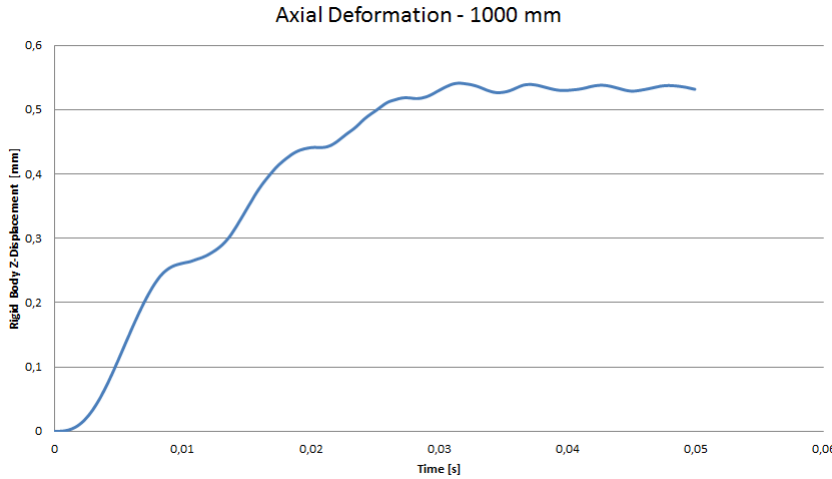

Figure 55: Axial deformation of left rigid plate - 1000 mm - Model 4

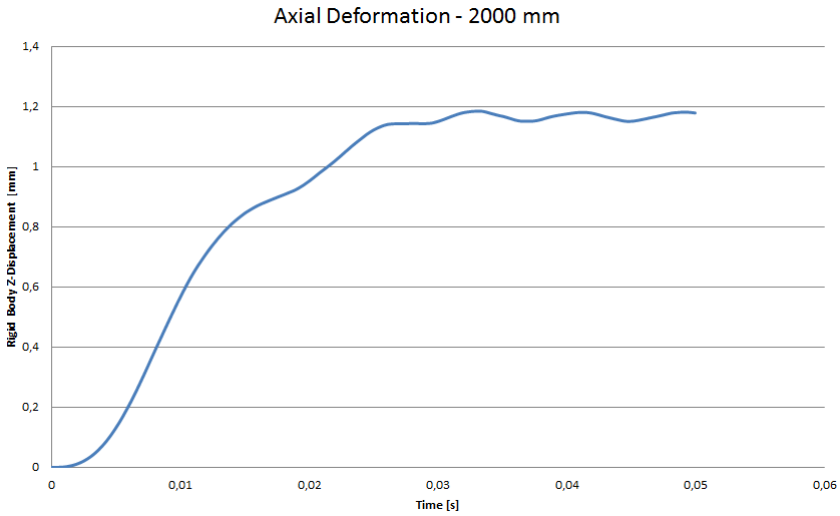

Figure 56: Axial deformation of left rigid plate - 2000 mm - Model 4

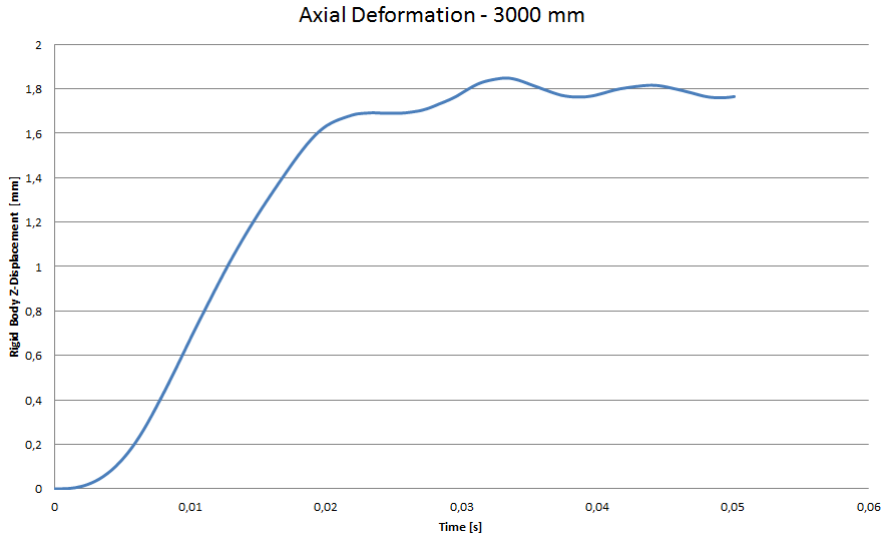

Figure 57: Axial deformation of left rigid plate - 3000 mm - Model 4

4.4.2 Bending stiffness

The results from the bending stiffness analyses are presented in the table below, where the bending stiffness values found are average values from the ramped load between load step 2 and load step 3.

Load step/Analysis	1000 mm	2000 mm	3000 mm
Δ M [kNm]	2,50	2,21	2,06
$k_{bending}$ [kNm^2]	26,22	23,78	27,23

Table 27: Results from the bending stiffness analyses - Model 4

The Y-directional deformation and the system energies of the three different cable lengths analysed are presented in the following figures.

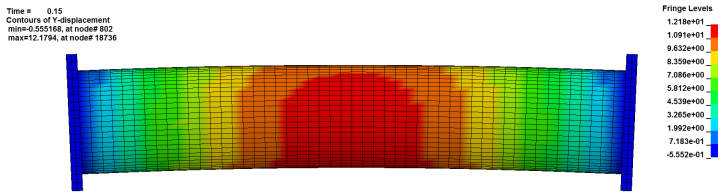

Figure 58: Y-Directional deformation at end time - 1000 mm - Model 4

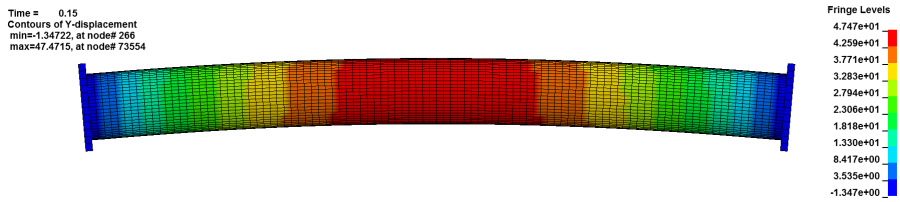

Figure 59: Y-Directional deformation at end time - 2000 mm - Model 4

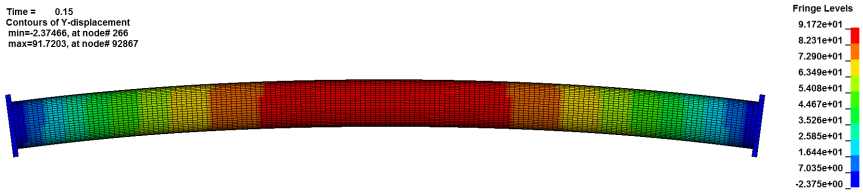

Figure 60: Y-Directional deformation at end time - 3000 mm - Model 4

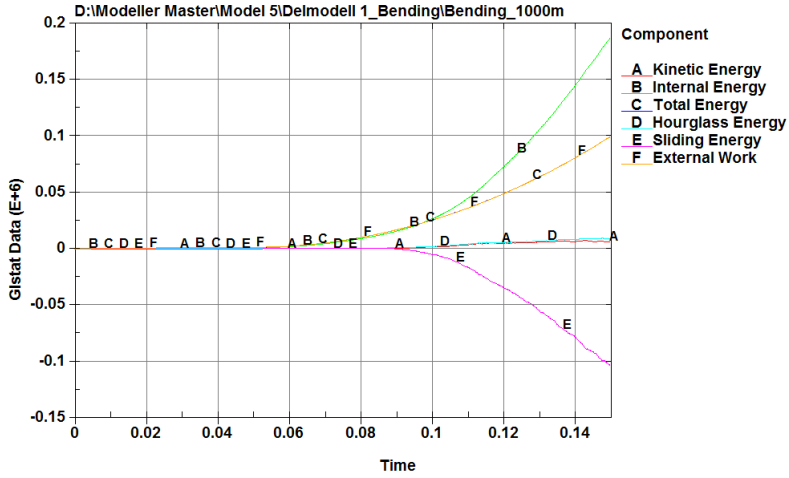

Figure 61: System energies, all bodies - 1000 mm - Model 4

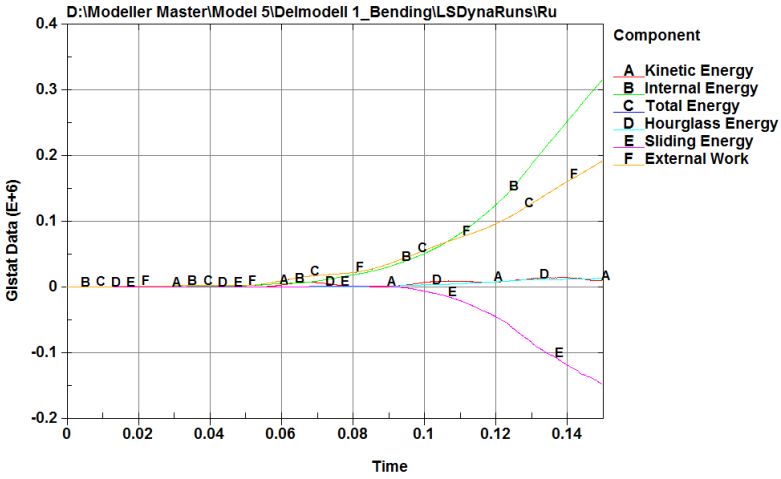

Figure 62: System energies, all bodies - 2000 mm - Model 4

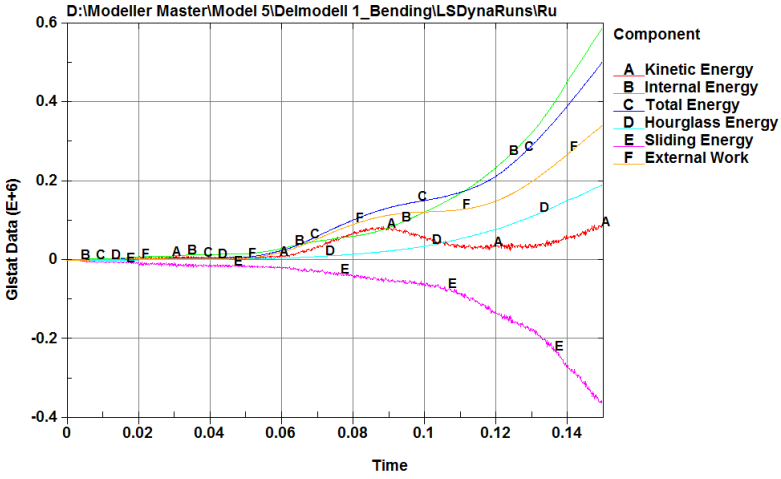

Figure 63: System energies, all bodies - 3000 mm - Model 4

4.4.3 Torsional stiffness

Based on the applied load steps presented in section 3.6.4, these are the following results from the torsional stiffness analyses:

Analysis	**1000 mm**	**2000 mm**	**3000 mm**
$\Delta\ \theta_{torsion}$ [Rad/m]	0,05236	0,05236	0,05236
$\Delta\ M_{torsion}$ [kNm]	7,35	6,69	9,81
$k_{torsion}$ [kNm^2]	140,56	128,06	187,38

Table 28: Results from the torsional stiffness analyses - Model 4

Figure 64 shows how the cable end is rotated at the end time, and how the middle part of the cable is deformed with respect to the fringe level at the right side.

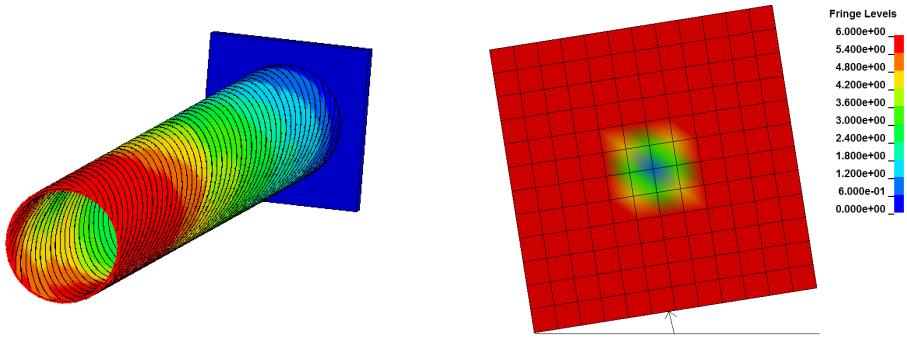

Figure 64: Total deformation at end time - 3000 mm - Model 4

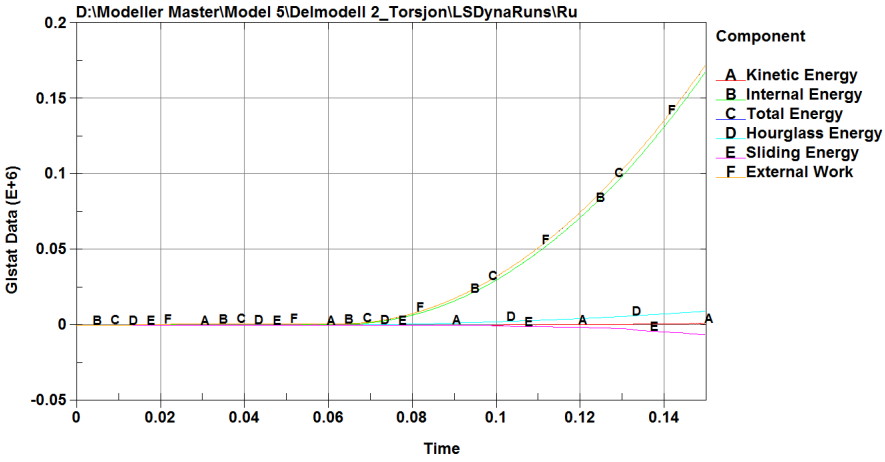

Figure 65: System energies, all bodies - 1000 mm - Model 4

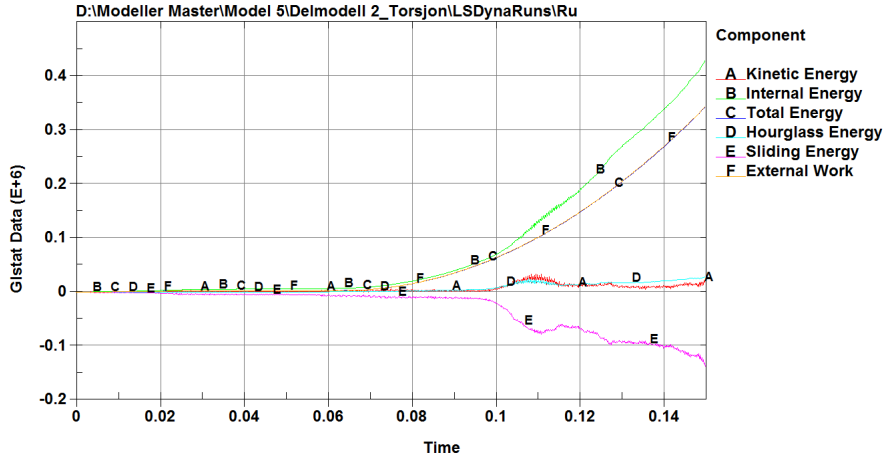

Figure 66: System energies, all bodies - 2000 mm - Model 4

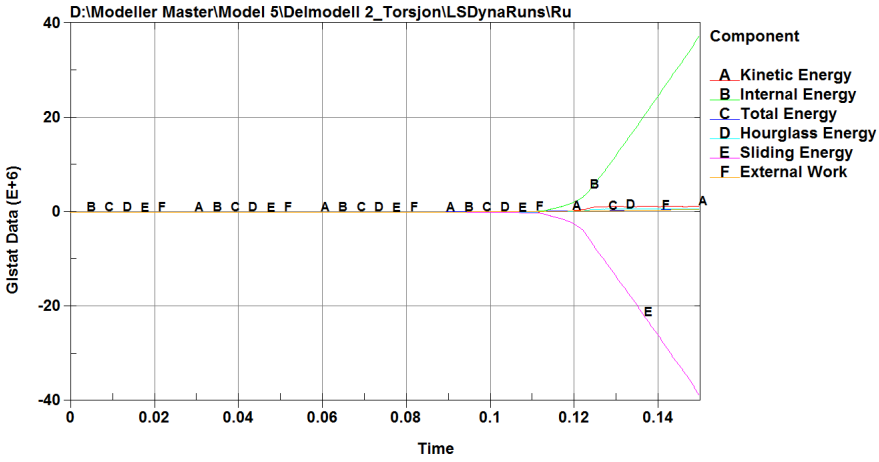

Figure 67: System energies, all bodies - 3000 mm - Model 4

4.5 Solve time statistics

Common for all the analyses done is that they have all been run with a program controlled memory allocation and with 6 CPU cores.

4.5.1 Model 1

Analysis	2000 mm	4000 mm	6000 mm
Axial stiffness	00:07:37	00:13:51	00:13:40
Bending stiffness	00:30:29	01:00:35	01:15:17
Torsional stiffness	00:14:12	00:25:25	00:23:26

Table 29: Run time statistics for the analyses performed of model 1

The analyses of axial- and torsional stiffness have been run with single solver precision, while the bending stiffness analyses have been run with double solver precision.

4.5.2 Model 4

Analysis	1000 mm	2000 mm	3000 mm
Bending stiffness	03:52:04	07:38:38	09:36:42
Torsional stiffness	04:09:33	06:47:39	10:06:48

Table 30: Run time statistics for the analyses performed of model 4

The run times of the bending stiffness- and torsional stiffness analyses include the pre-tension load step, i.e. there has not been performed any re-start analyses.

4.6 Discussion

Model 1 Analysing model 1 shows that ANSYS LS-Dyna gives good results when handling such a simple model as a flexible cable of structural steel. Independent of the cable lengths analysed, the results of the global stiffness parameters were good. This was particularly evident for the analyses of the bending stiffness, where the results were more or less equal to the theoretical bending stiffness.

Results from this model gives good indication of that ANSYS-LS dyna is capable of handling such slender structures with an explicit approach within a loading time interval of only 0,1 seconds. The CPU times presented in section 4.5 are also considered reasonable, with the longest run time of 01:15:17 for the cable of six meter.

Model 2 This model indicated that the contact tools of ANSYS LS-Dyna works properly, and that can give good results when analysing frictional behavior between two flexible solid bodies. Several run were done, which led to the conclusion that the load step set up was of high importance. If not, the box started to slide or stick to the plate when it was not suppose to. Therefor, this auxiliary model was of great help when modeling Model 2, a model developed to investigate exactly this issue. Only then the frictional behavior of interest were between the wound tendon and the coating during bending.

Model 3 An initially requirement was that the tendon had to be in the stick domain before the bending could start, hence several pre-tension values were tested before the final analysis were run. Initially the pretension of 100 kN was to high, resulting in the tendon to penetrate and squeeze the inner cover of polyethylene. This is illustrated in figure 68.

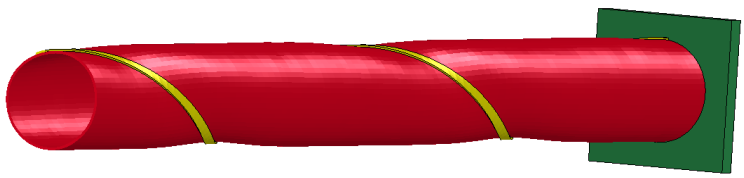

Figure 68: To high pre-tension - Model 3

In the end, the cable was subjected to a pre-tension force of only 5 kN which was enough to get the tendon to stick to the inner cover and without effecting the

geometry of it. The cable length analysed was chosen to be four meters. In this way it was possible to analyse and capture the behavior of the wound tendon at the mid point of the cable without the influence of any possible end effects.

Based on theory and the analysis of this model gave results indicating that there do exist a stick/slip points after only 0,03 second of bending. But, further work should still be done in this matter to be 100 % sure that this conclusion is valid.

Model 4 If assuming there do exist a distinct stick-slip point during bending, this does not seem to influence the ability to calculate the bending stiffness. Three cables where analysed, and all three of them gave bending stiffness values in the same range. Also, the values found for the axial stiffness analyses gave good results. Hence, the change in cable length did not effect the outcome of this analysis. But, the analyses of the torsional stiffness did not give as consistent results as desired, having a value range of 59,32 kN in total.

The longest CPU time was 10:06:48, and was from the torsion stiffness analysis of the three meter long cable.

There were not found any correlation between a lay angle below $\alpha = 20°$ and the ability to run a bending analysis without the tendons spreading appart like they do in the figure below. But again, the observations done looking for this correlation should be part of further work done.

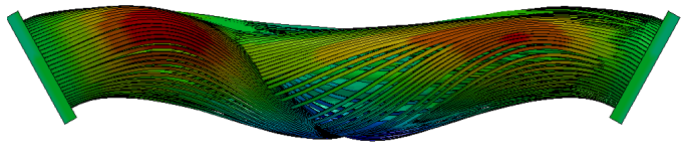

Figure 69: Tendons spreading during bending

References

[1] M.A. Vaz A.B. Custódio. A nonlinear formulation for the axisymmetric response of umbilical cables and flexible pipes. *Applied Ocean Research*, 24:21–29, 2002.

[2] ANSYS. *ANSYS 14.5 Help System*.

[3] ANSYS. *Introduction to ANSYS Explicit STR & Introduction to ANSYS Autodyn Part I, Lecture 7, Explicit Meshing*, November 1 2012.

[4] Robert D. Cook. *Concepts and Applications of Finite Element Analysis, 4th ed.* John Wiley & Sons, inc., 2007.

[5] J.-M. Leroy and P.Estrier. Calculation of stresses and sslip in helical layers of dynamically bent flexible pipes. *Oil & Gas Science and Technology*, 56:545–554, 2001.

[6] D. Margolis. Fixed causality slip-stick friction models for use in simulations of non-linear systems. *System and Control Engineering*, 219 part I:7, 2005.

[7] S. Sævik and J. K. Ø. Gjøsteen. Strength analysis modelling of flexible umbilical members for marine structures. *Applied Mathematics*, 2012:18, 2013.

[8] Svein Sævik. A finite element model for prediciting stresses and slip in flexible pipe armouring tendons at bending gradients. *Computers and Structures*, 46:2:2273–2291, 1993.

[9] Svein Sævik. Theoretical and experimental studies of stresses in flexible pipes. *Computers and Structures*, 89:2273–2291, 2011.